

NEURAL NETWORKS PREDICT WELL INFLOW PERFORMANCE

A Thesis

by

MUHAMMAD ALRUMAH

Submitted to the Office of Graduate Studies of
Texas A&M University
in partial fulfillment of the requirements for the degree of
MASTER OF SCIENCE

December 2003

Major Subject: Petroleum Engineering

NEURAL NETWORKS PREDICT WELL INFLOW PERFORMANCE

A Thesis

by

MUHAMMAD ALRUMAH

Submitted to the Office of Graduate Studies of
Texas A&M University
in partial fulfillment of the requirements for the degree of

MASTER OF SCIENCE

Approved as to style and content by:

Richard Startzman
(Co-Chair of Committee)

David S. Schechter
(Co-Chair of Committee)

Wilbert E. Wilhelm
(Member)

J. Bryan Maggard
(Member)

Hans C. Juvkam-Wold
(Head of Department)

December 2003

Major Subject: Petroleum Engineering

ABSTRACT

Neural Networks Predict Inflow Performance. (December 2003)

Muhammad Alrumah, B.S., Kuwait University

Co-Chairs of Advisory Committee: Dr. Richard Startzman
Dr. David S. Schechter

Predicting well inflow performance relationship accurately is very important for production engineers. From these predictions, future plans for handling and improving well performance can be established. One method of predicting well inflow performance is to use artificial neural networks.

Vogel's reference curve, which is produced from a series of simulation runs for a reservoir model proposed by Weller, is typically used to predict inflow performance relationship for solution-gas-drive reservoirs. In this study, I reproduced Vogel's work, but instead of producing one curve by conventional regression, I built three neural network models. Two models predict the IPR efficiently with higher overall accuracy than Vogel's reference curve.

DEDICATION

All Praise be to Allah, Cherisher and Sustainer of Worlds, who bestowed me with life and health to complete this work.

I wish to dedicate this work to my mother and father for their continuous prayer and patience.

I dedicate this work to my brothers and sisters for their encouragement.

I dedicate this work to my wife for her sacrifices of her health and time to provide me with a suitable environment. Her patience and encouragement was the drive for me.

I dedicate this work to my son, Yousuf, whose smile is the hope and whose laugh is the bright future.

ACKNOWLEDGMENTS

I would like to express my appreciation for the assistance and suggestions of my thesis committee members including Dr. Richard Startzman, co-chair, Dr. David Schechter, co-chair, Dr. Bryan Maggard, and Dr. Wilbert Wilhelm.

I would like to extend my appreciation to Dr. Stuart Scott for allowing me to use his lab.

Special thanks go to those who provided me with continued support and help, Mazher Ibrahim, Mohamed El-Ahmady, and Ahmed Daoud.

Finally, I want to thank the faculty and staff of the Department of Petroleum Engineering at Texas A&M University and all my colleagues.

TABLE OF CONTENTS

	Page
ABSTRACT.....	iii
DEDICATION	iv
ACKNOWLEDGMENTS.....	v
TABLE OF CONTENTS	vi
LIST OF TABLES	vii
LIST OF FIGURES.....	viii
INTRODUCTION.....	1
BACKGROUND.....	3
Inflow Performance Relationship	3
Artificial Neural Network	7
MODEL DEVELOPMENT	10
Reservoir Model.....	10
Comments on Vogel's Work.....	23
Neural Network Models.....	25
MODEL EVALUATION AND DISCUSSION	34
CONCLUSIONS.....	52
NOMENCLATURE.....	54
REFERENCES.....	56
APPENDIX	58
VITA	66

LIST OF TABLES

TABLE		Page
1	Reservoir properties and descriptions.	11
2	Relative permeability and PVT curves selected for cases examined.....	19
3	Sample of results from reservoir simulation	22
4	The weights for first neural network model.....	28
5	Threshold for first neural network model.	28
6	The weights for second neural network model	30
7	Threshold for second neural network model.....	30
8	The weights for third neural network model.....	33
9	Threshold for third neural network model	33

LIST OF FIGURES

FIGURE	Page
1 Basic structure for multilayer perceptron network.....	8
2 Relative permeability curves.....	13
3 R_s curves.....	14
4 μ_o curves.....	14
5 B_o curves.....	15
6 $1/B_g$ curves.	15
7 μ_g curves.....	16
8 IPR curves generated from simulator for gridblock sensitivity.	17
9 IPR curves for case 1 (refer to Table 2).	20
10 Relative change in productivity index with time.	21
11 PVT curves from Vogel's paper	24
12 Relative permeability curves from Vogel's paper.	24
13 Illustration for the construction of the first neural network model.	27
14 Illustration for the construction of the second neural network model.	30
15 Illustration for the construction of the third neural network model.....	32
16 Percentage relative error of the predicted q_o for training data (first model) ...	36
17 Percentage relative error of the predicted q_o for evaluation data (first model versus Vogel's equation)	37

FIGURE	Page
18 Percentage relative error of the predicted q_o for training data (Vogel's equation)	38
19 Comparing the IPR curves produced using the first model and Vogel's equation to the actual IPR curves	39
20 Crossplot for q_o for training data (first model).....	40
21 Dimensionless IPR for actual, second model, and Vogel's equation	41
22 Percentage relative error of the predicted $q_o/q_{o\max}$ for training data (second model)	42
24 Percentage relative error of the predicted $q_o/q_{o\max}$ for training data (Vogel's equation).....	44
23 Percentage relative error of the predicted $q_o/q_{o\max}$ for evaluation data (second model versus Vogel's equation)	43
25 Crossplot for $q_o/q_{o\max}$ for training data (second model).....	45
26 Percentage relative error of the predicted q_o for training data (third model) ..	46
27 Percentage relative error of the predicted p_r for training data (third model) ..	47
28 Percentage relative error of the predicted q_o for evaluation data (third model).....	48
29 Percentage relative error of the predicted p_r for evaluation data (third model).....	49
30 Crossplot of q_o for training data (third model).....	50
31 Crossplot of p_r for training data (third model)	51

INTRODUCTION

The inflow performance relationship (IPR) describes the relationship between well flow rate and bottomhole pressure. IPR helps petroleum engineers to optimize production, identify the optimal design for artificial lift, and predict future production following a stimulation treatment.

Vogel¹ built a simulation model using Weller's² assumptions for solution-gas-drive reservoirs. Vogel¹ produced IPR curves for different cases, and then plotted dimensionless IPR curves for these cases. Noticing that most of these curves exhibited the same behavior, he used regression to derive an equation that related flow rate to flowing bottomhole pressure in an equation for a curve.

Artificial neural networks have been widely used³ and are gaining attention in petroleum engineering because of their ability to solve problems that previously were difficult or even impossible to solve. Neural networks have particularly proved their ability to solve complex problems with nonlinear relationships.

Shippen⁴ developed a neural network model for prediction of liquid holdup in two-phase horizontal flow and the results exhibited better overall performance than other existing methods.

Zambrano⁵ developed a neural network model to predict dewpoint pressure for retrograde gases; the model showed better estimation than all existing correlations.

This thesis follows the style of the *Journal of Petroleum Technology*.

An artificial neural network is a network that simulates the learning processes in the human brain. It builds its own model on the basis of given information, and then estimates an output from new input. The network consists of neurons and connections between them. In neural network language, we call the connections weights. Specific values are stored in those weights to simulate the human brain. The main advantage of the neural network is that it can learn from given input and output and establish its own model and relationships between output and input to estimate future values.

I used the neural network to build three models. Two models are able to establish the IPR curve with an overall accuracy better than Vogel's equation and with a reasonable accuracy for the third model. The first model predicts the oil flow rate by providing more than one input to indicate the IPR curve more specifically. The second model predicts the $q_o/q_{o\max}$. This model has more accurate results than the first model. The third model predicts the oil flow rate and the average reservoir pressure.

BACKGROUND

Inflow Performance Relationship

The relationship between flow rate (q) and the flowing bottomhole pressure (p_{wf}) is described with an equation for easier analysis for well performance. One of the earliest attempts for establishing this relationship was based on the assumption that the flow rate is directly proportional to the pressure drawdown; the relationship can be derived from Darcy's law for steady-state flow and a single, incompressible fluid. The straight line equation in equation form is

$$q = J(p_e - p_{wf}), \dots\dots\dots (1)$$

where J is the productivity index and p_e is the pressure at the outer boundary.

But this wasn't the case in a two-phase gas and oil reservoir. Evinger⁶ pointed out that for a gas and oil flowing in the reservoir, a single J value cannot be assigned; rather, it will vary. Hence the IPR will exhibit a curvature indicating varying J value with changing pressure as J is a function of pressure/volume/temperature, rock properties, and relative permeability.

Vogel¹ used a numerical simulation to investigate the behavior of the IPR of a solution-gas-drive reservoir producing below the bubblepoint pressure. He generated

IPR curves for 21 fictitious solution-gas-drive reservoirs that covered different fluid PVT properties and relative permeability characteristics.

Vogel¹ plotted the different IPR curves as dimensionless IPR curves, where for a particular curve the pressure was divided by the maximum or shut-in pressure, and the corresponding flow rate was divided by the maximum flow rate. When he noticed that the curves were generally exhibiting a similar shape, he applied regression analysis to find the best curve that can represent all curves. A dimensionless IPR curve could be used to create the IPR curve for any well that produces from a solution-gas-drive reservoir at any depletion stage, using only a one-point test. The equation for this dimensionless IPR curve is

$$\frac{q_o}{q_{o\max}} = 1 - 0.2 \frac{p_{wf}}{p_r} - 0.8 \left(\frac{p_{wf}}{p_r} \right)^2, \dots\dots\dots (2)$$

Vogel didn't include IPR curves for wells with damage or high viscosity because the dimensionless curves for them deviated significantly from curves for undamaged wells and lower oil viscosity.

Fetkovich⁷ found that the back-pressure curves for the data collected from saturated and undersaturated reservoirs follow the same general form as that used for gas wells:

$$q = C(p_r^2 - p_{wf}^2)^n, \dots\dots\dots (3)$$

where n is the exponent of back-pressure curve.

Flow Efficiency and Skin Effect. Standing⁸ extended Vogel's dimensionless IPR curves to different flow efficiencies, defining flow efficiency as the ratio of the flow rate without damage to the flow rate with damage. Standing⁸ assumed this definition was valid for two-phase system.

Brown⁹ showed that Standing's method will give inconsistent results for high flow efficiency and low flowing bottomhole pressure. The cause of the inconsistent results was pointed out by Camacho and Raghavan¹⁰, who showed that as Vogel's IPR suggests a quadratic form for deliverability, it implies that the definition of flow efficiency must also reflect the quadratic form of the deliverability equation instead of the straight line definition.

Camacho and Raghavan¹⁰ used numerical simulation in a theoretical study to investigate the effects of skin on well performance producing from solution-gas-drive reservoirs. They showed that skin does not change the deliverability curve from quadratic into linear form.

Klins¹¹ also reached the conclusion that a dimensionless IPR curve will not be affected if skin is present. He investigated the factors that affect the dimensionless IPR behavior and concluded that the bubblepoint pressure and reservoir depletion had a significant effect.

Inflow Performance Relationship Prediction. For predicting the IPR curve, Standing¹² presented an extension for Vogel's IPR equation that can predict the future IPR curve for the well as a result of change in $\left(\frac{k_{ro}}{B_o\mu_o}\right)$. Fetkovich⁷ also developed a method to predict the future IPR by relating the current average reservoir pressure to the future average reservoir pressure. These two methods assumed that the $\left(\frac{k_{ro}}{B_o\mu_o}\right)$ relation changes linearly with respect to pressure.

Camacho and Raghavan¹⁰ determined that the two methods can be used for IPR prediction, but that extrapolations over long periods of time should be avoided.

This Work. I created several IPR curves from simulation runs using the ECLIPSE™ simulator for a solution-gas-drive reservoir model with different rock and PVT properties and relative permeability characteristics. I used these results to build three artificial neural network models that can generate and predict IPR curves.

Artificial Neural Network

The artificial neural network is a mathematical model that is designed to replicate the learning capabilities of biological neural systems by modeling the low-level structure of the brain. It has been used for solving problems that previously were difficult or even impossible to solve.

Biological Neural Network. The artificial neural network was inspired by the information process in the human brain, where it processes the information in a way entirely different than conventional computer models. The brain is a highly complex, nonlinear and parallel computer (information-processing system) that has the capability to perform certain computations many times faster than the fastest digital computer¹³.

Artificial Neural Network. The artificial neural network is a simulation model for the most basic learning process of the human brain. The network is constructed as interconnected neurons; simple processing units that receive and combine signals. The information is transported from neuron to neuron through a connection or a weight, in neural network terms.

Haykin¹³ identified three fundamentally different classes of network architectures: single-layer feedforward networks, multilayer feedforward networks, and recurrent networks. No single neural network works better for all types of problems. The multilayer perceptron (MLP) is the most common network used in the petroleum

industry^{4,5}. The structure for the MLP consists of an input and output layers and at least one hidden layer. Each layer consists of number of nodes, depending on the problem (Fig. 1).

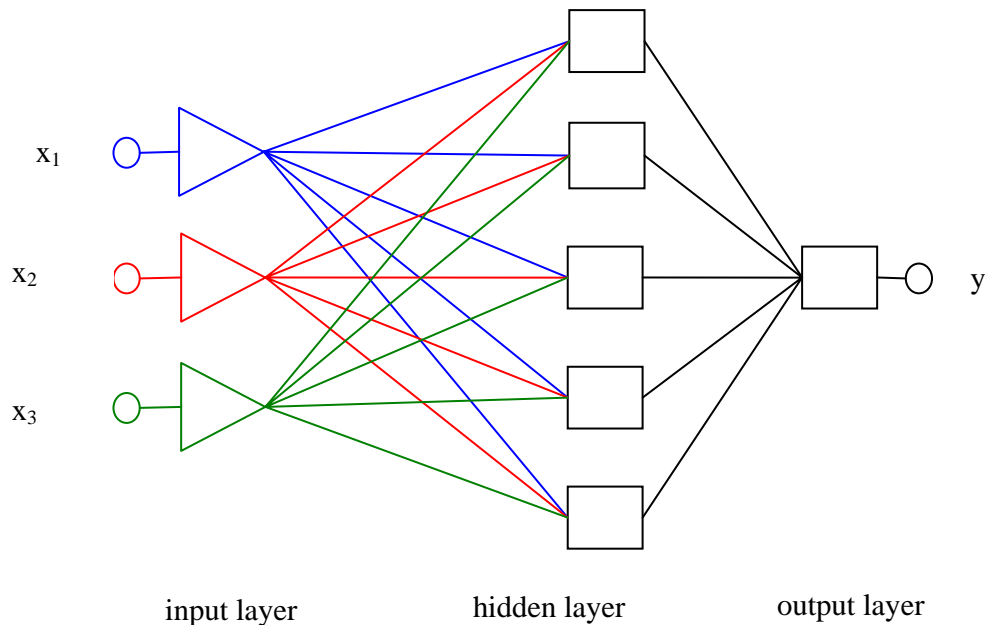


Fig. 1 Basic structure for multilayer perceptron network

In the feedforward network, each neuron in each layer except the input and the output layers is connected to all neurons of the preceding and the following layer, and there is no connection between the neurons in the same layer. This connection pattern ensures that the network outputs can be calculated as explicit functions of the inputs and the weights¹³. The information given to the input layer is propagated layer by layer to the output layer through one or more hidden layers.

Choosing Neural Network Structure. The first step for building neural network model is to design the network structure. The basic structure for a multilayer perceptron is at least three parallel layers, where each layer has at least one node. The nodes in the layers are connected with each other in feedforward pattern. Three layers are sufficient to learn any continuous function as it is directly applicable to the universal approximation theorem¹³.

In the input layer, each node represents a parameter that has a relationship with the output; the output layer contains the number of parameters we need to predict. Number of nodes in the hidden layer can't be determined easily. Instead, it is an iterative process, where we need to try different number of nodes and then compare the results to see which the best structure is.

Learning. The neural network can learn in either of two ways; either we can feed the system the input data and the actual output, or we can allow the system to group similar inputs into classes. Once the system has reached satisfactory results with a set of training data, it can process new information in the same way to reach the same logical end. I used the first of these ways.

MODEL DEVELOPMENT

Reservoir Model

I examined the ability of the neural network to build a model that can establish and predict well inflow performance for solution-gas-drive reservoirs. In the learning process, the neural network used input and output data together taken from reservoir simulation models to construct a neural network model. Then the model predicted the output from only the input.

I built several simple solution-gas-drive reservoir models with only one producing vertical well and the following assumptions were considered for simplification,

- 1- The well is centered in a cylindrical, homogeneous, and isotropic reservoir.
- 2- The oil zone is one layer and has constant thickness for the whole reservoir.
- 3- The reservoir is completely bounded.
- 4- The well is completely penetrating the oil zone.
- 5- The initial water saturation is at the connate water saturation.
- 6- Gravity and capillary pressure effects were neglected.

Table 1 lists the reservoir properties and descriptions, which are taken from Vogel's paper¹.

Table 1 - Reservoir properties and descriptions	
Porosity (ϕ)	13.9%
Permeability (k)	20 md
Formation thickness (h)	23.5 ft
Well radius (r_w)	0.33 ft
Outer radius (r_e)	527 ft
Irreducible water saturation (S_{wc})	19.4%

The IPR for solution-gas-drive reservoir above bubblepoint pressure can be presented as a straight line with constant productivity index (J). The IPR straight line equation can be described as follows:

$$q = J(p_e - p_{wf}), \dots\dots\dots (1)$$

and

$$J = \frac{q}{(p_e - p_{wf})} = \frac{7.08 \times 10^{-3} kh}{\mu_o B_o \left(\ln \frac{r_e}{r_w} \right)}, \dots\dots\dots (4)$$

These equations can be derived from Darcy's law for steady-state flow and a single, incompressible fluid. However, below the bubblepoint pressure there will be two phases flowing, gas and oil. The oil productivity index will change with the change of pressure because the oil properties and relative permeabilities are changing.

I investigated well performance relationship below the bubblepoint. For that, the initial reservoir pressure always starts at the bubblepoint pressure for all the simulation runs. Hence, the well is produced at a flowing bottomhole pressure below bubblepoint pressure.

Fluid and Rock Properties. I used different fluid properties and relative permeability curves taken from Vogel's paper¹ to cover a wide range of cases (see **Figs. 2 through 7**).

The porosity and absolute permeability remained constant for all the cases.

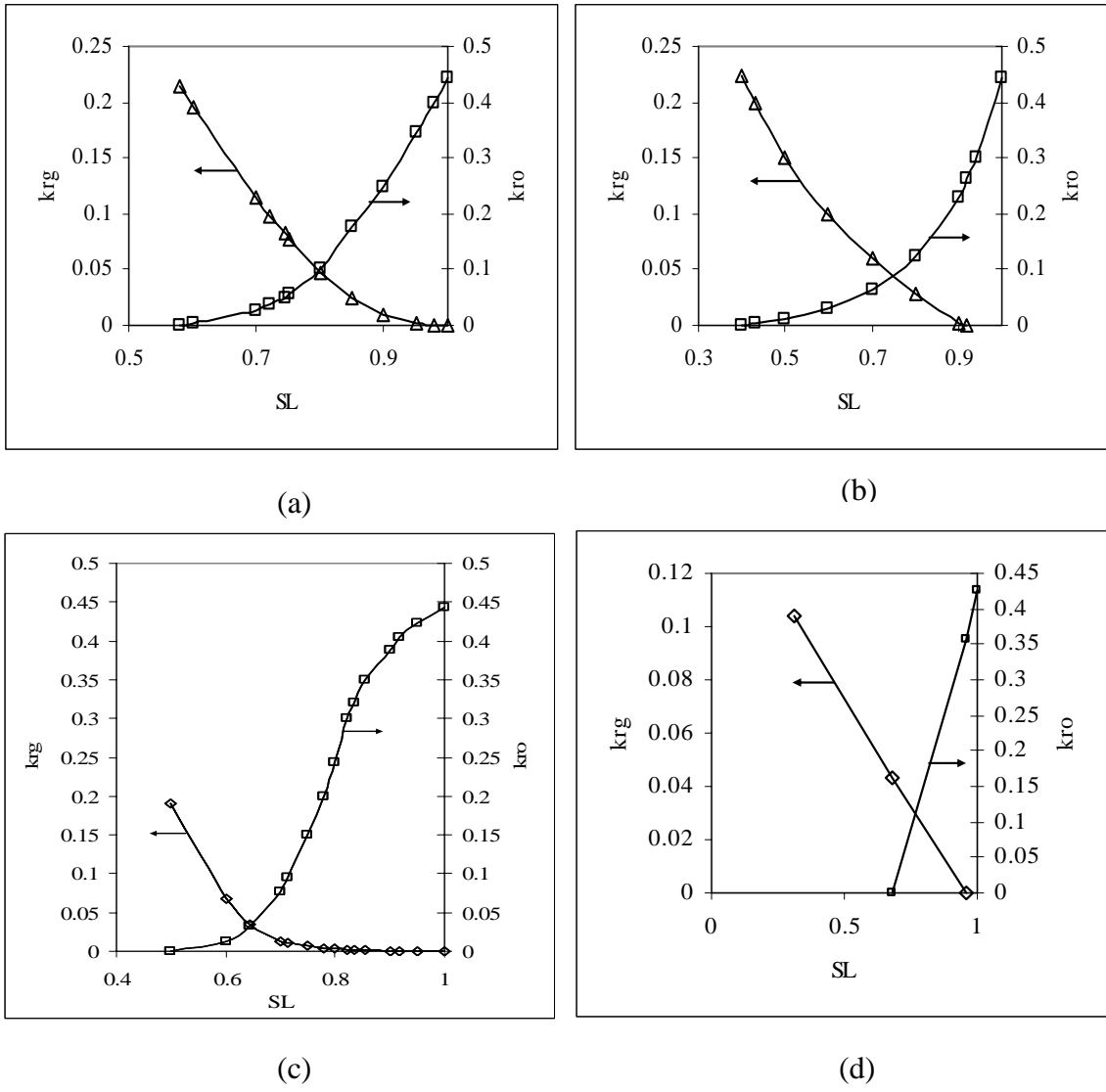


Fig. 2 Relative permeability curves

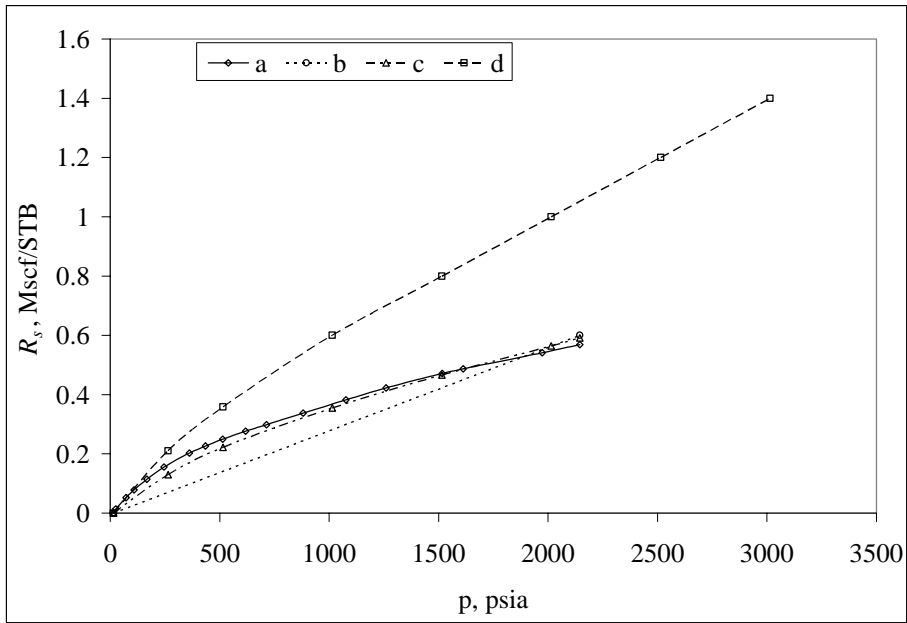


Fig. 3 R_s curves

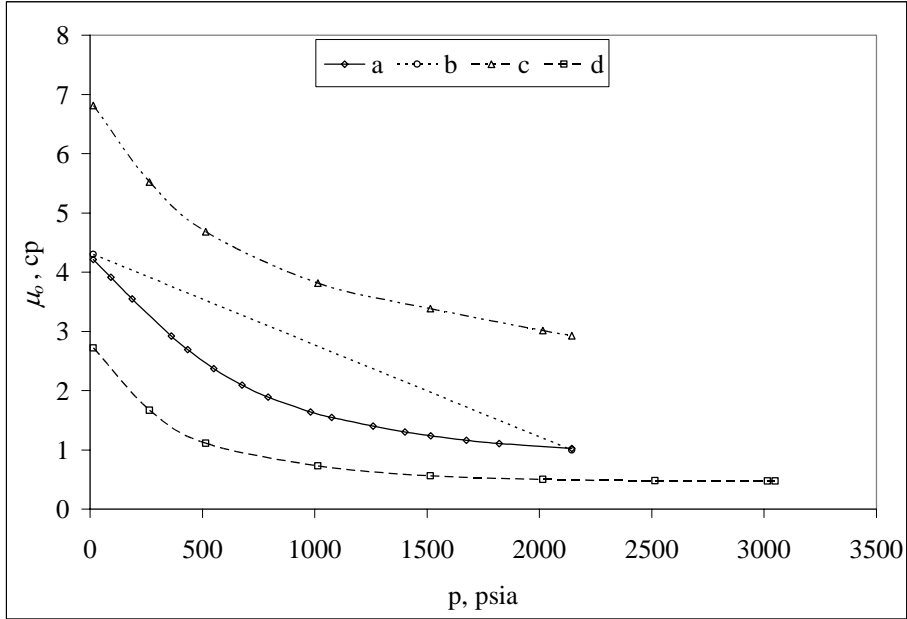


Fig. 4 μ_o curves

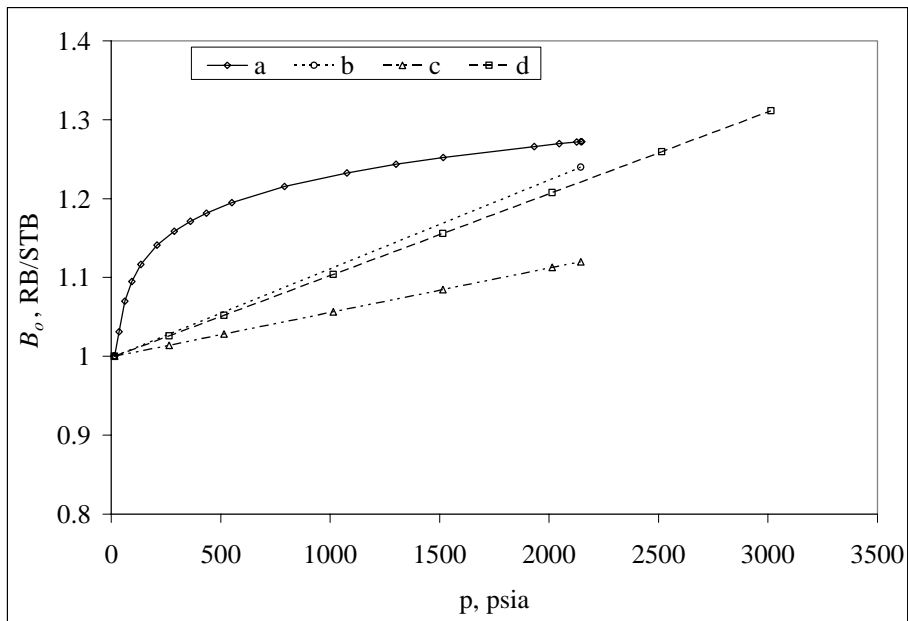


Fig. 5 B_o curves

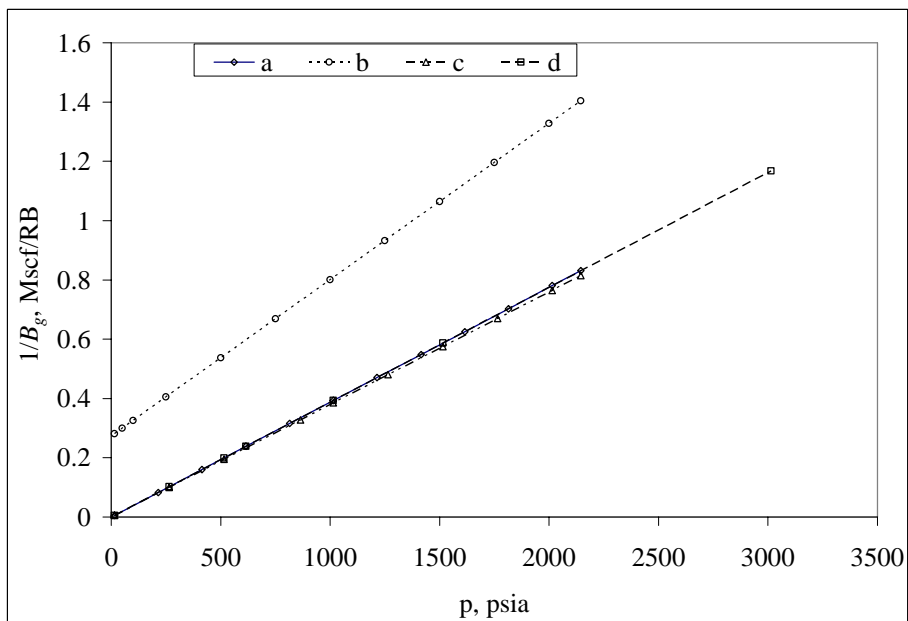


Fig. 6 $1/B_g$ curves

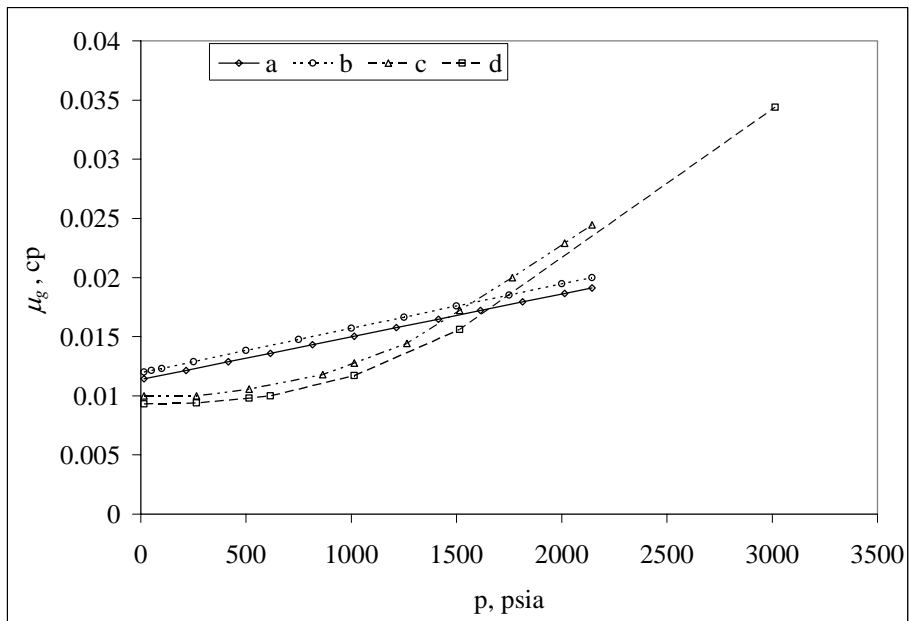


Fig. 7 μ_g curves

Model Accuracy. Before performing the simulation runs, I had to decide which grid size is best to use for the reservoir to get results with reasonable accuracy.

I was not concerned about a high degree of accuracy because the aim was to produce the trend of the relationship between the flow rate and the flowing bottomhole pressure. Three values for grid sensitivity were examined in the 1-D simulation; 10, 100 and 1,000 gridblock. For each grid size I ran the simulation and produced IPR curves.

Fig. 8 shows the IPR curves for the different grid sizes. All three curves are similar below 50 STB/D, but above it the curve for 10-grids starts to deviate from the other two.

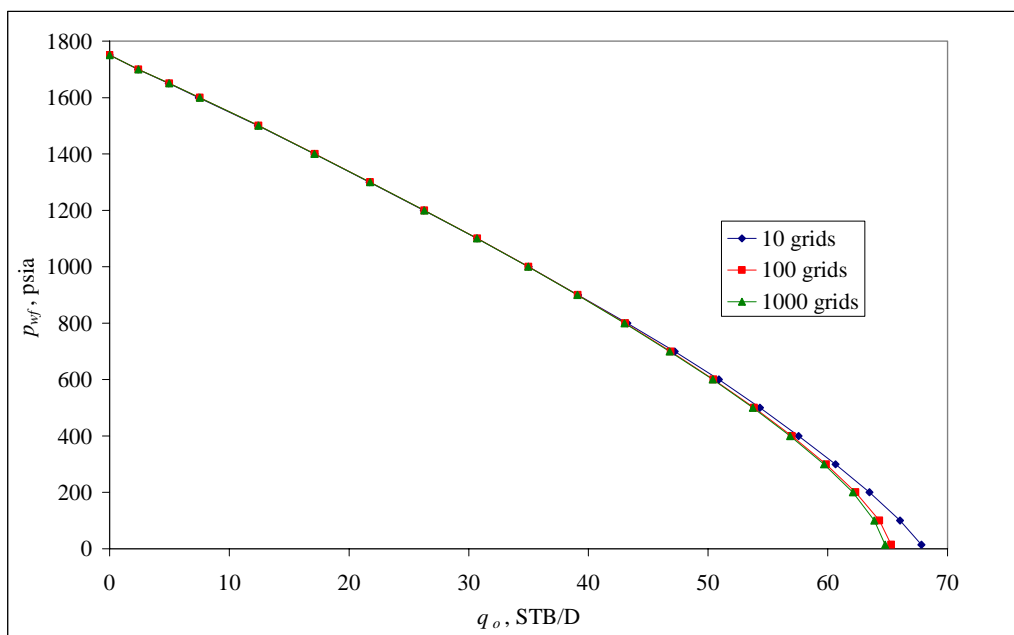


Fig. 8 IPR curves generated from simulator for gridblock sensitivity

I chose the 100-grid size because it has much less computational time than the 1000-grid size, as the computational time increases with increasing number of grids. The reservoir was divided into radial grids and the radii were calculated from the following equation:

$$r_i = r_w \left(\frac{r_e}{r_w} \right)^{i/NR}, \dots\dots\dots (5)$$

where NR is total number of grids and i is the index number. This made the gridblocks adjacent to the wellbore small enough to permit capturing the change in pressure and saturation. The gridblocks then increase progressively in size outward from the wellbore, because as the radius increases, the gradients in pressure and saturation are lower and bigger gridblocks are sufficient to capture these changes.

Reservoir Model Results. The first phase of this work produced families of IPR curves for different fluid properties and relative permeability curves as these are the main parameters affecting the IPR curves.

IPR curves were generated for 16 reservoir models. The relative permeability and PVT for the cases examined are tabulated in **Table 2**.

Table 2 – Relative permeability and PVT curves selected for cases examined		
Case no.	Relative permeability curve	PVT curves
1	a	a
2	b	a
3	c	a
4	d	a
5	a	b
6	b	b
7	c	b
8	d	b
9	a	c
10	b	c
11	c	c
12	d	c
13	a	d
14	b	d
15	c	d
16	d	d

The IPR curves generated from a reservoir simulation runs for case 1 depicted in **Fig. 9**. The IPR curves for the remaining cases are in Appendix.

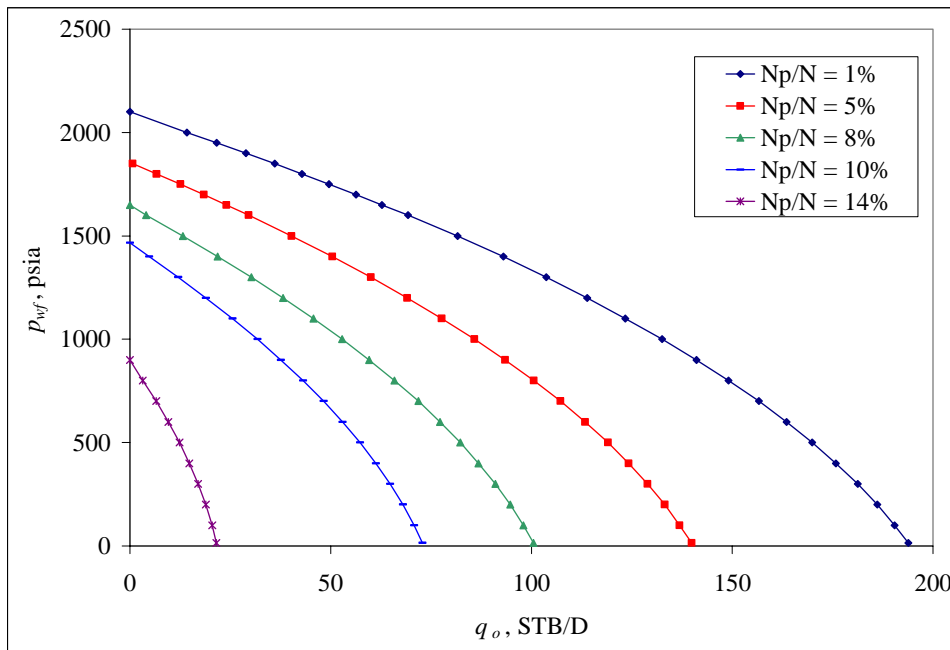


Fig. 9 IPR curves for case 1 (refer to Table 2)

For each case with specific fluid properties and relative permeability curves, I made several runs at constant bottomhole pressure. The results include time with the corresponding oil flow rate (q_o) and the cumulative oil produced (N_p).

The reservoir model didn't reach constant productivity index to achieve the boundary dominated flow condition, but for practical purposes, I assumed the condition was reached when I get a relative change in the productivity index less than 1% (**Fig. 10**).

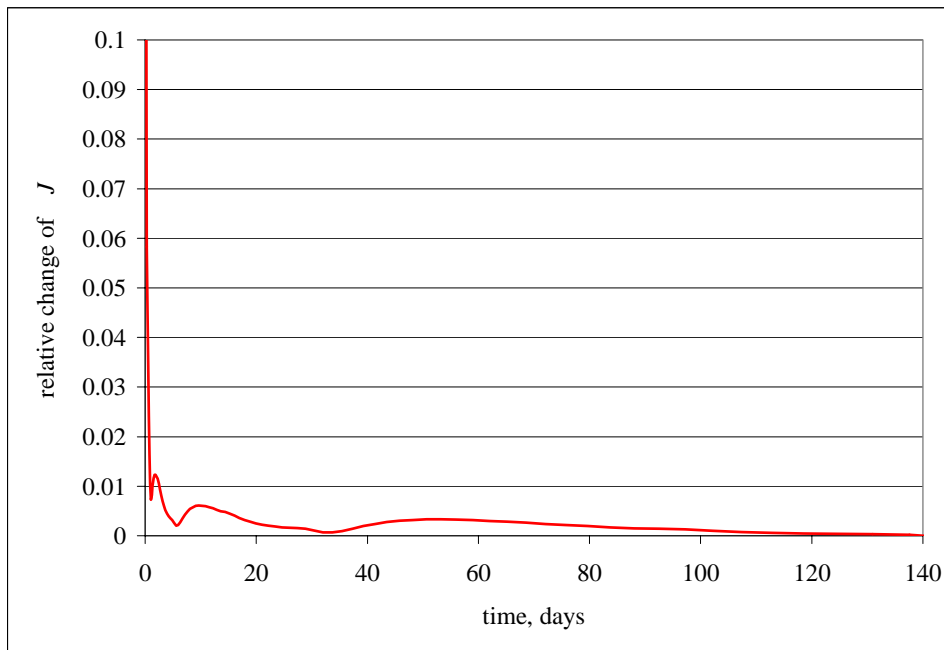


Fig. 10 Relative change in productivity index with time

To draw a single IPR curve, first we choose a single specified value for the cumulative produced oil (N_p) and at that chosen value we read the corresponding production rate from each run. At the end, a table of q_o with p_{wf} will be established for the chosen N_p . This procedure is repeated for different N_p values. An example procedure for calculating a single point on the IPR curve is shown as follows:

Using **Table 3**, we want to establish an IPR curve at $N_p = 50,000$ STB.

Table 3 – Sample of results from reservoir simulation					
$p_{wf} = 900$ psia		$p_{wf} = 800$ psia		$p_{wf} = 700$ psia	
q_o	N_p	q_o	N_p	q_o	N_p
STB/DAY	STB	STB/DAY	STB	STB/DAY	STB
31.32	47318	32.79	50014	34.65	52346
30.23	48917	31.45	52093	33.12	54061
29.06	50532	30.03	53767	31.39	55767
27.80	52153	28.45	55431	29.68	57461
26.49	53776	26.84	57081	27.85	59130
25.03	55385	25.22	58708	25.83	60755

For the simulation run for $p_{wf} = 900$ psia there is no value for $N_p = 50,000$ STB.

So we interpolate to get the corresponding oil flow rate as follows,

$$q_o (@ N_p = 50,000 \text{ STB}) = \frac{(29.06 - 30.23)}{(50,532 - 48,917)} * (50,000 - 48,917) + 30.23 = 29.44 \text{ STB} / D$$

This point will correspond to $p_{wf} = 900$ psia.

We perform the same procedure for $p_{wf} = 800$ psia and $p_{wf} = 700$ psia to have three points on the IPR curve of $N_p = 50,000$ STB

The best performance for the well will be at the early time of the reservoir life when there is high oil saturation and the average reservoir pressure (p_r) is high, and hence, gives high maximum oil flow rate. As the reservoir is being depleted, this reduces reservoir energy, and decreasing p_r . When p_r decreases, this causes more gas to evolve from solution to increase gas saturation and decrease oil saturation which will reduce the oil relative permeability, causing well performance to give lower oil flow rates.

When the reservoir is fully depleted, the family of IPR curves is produced. The IPR curves exhibit the shape of concave downward as N_p increases.

Comments on Vogel's Work

I tried to match Vogel's results with my results that were generated from the reservoir simulation using Vogel's data. The matching was unsuccessful.

I have the following notes about Vogel's data:

- Of the six PVT curves, five have the same bubblepoint pressure, which is 2130 psig, although they have different PVT properties.
- Most PVT curves were approximated as straight lines, which is unrealistic.
- At 14.7 psia, the value of $(1/B_g)$ equals 50, which cannot occur, in the PVT curve in **Fig. 11**. There was no clue about the units of $(1/B_g)$. So, I assumed it is (scf/rcf), which was the most reasonable unit.
- The k_{ro} curve stops before it intersects with the saturation axis at $k_{ro} = 0$. It doesn't show the minimum liquid saturation, SL (**Fig. 12**).

Vogel showed that the dimensionless IPR for a damaged well will nearly approach a straight line, with significant deviation for more viscous crude. But Klins¹¹ proved that neither damaged nor improved skin has significant effect on dimensionless IPR curve, and for more viscous crude, the dimensionless IPR curve exhibited a shape similar to the less viscous crude.

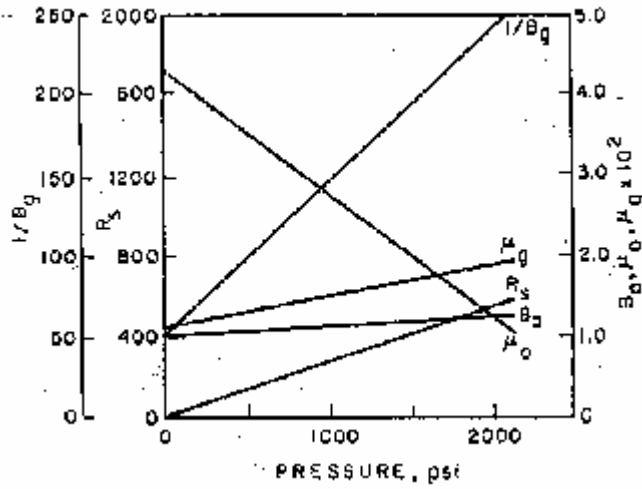


Fig. 11 PVT curves from Vogel's paper¹

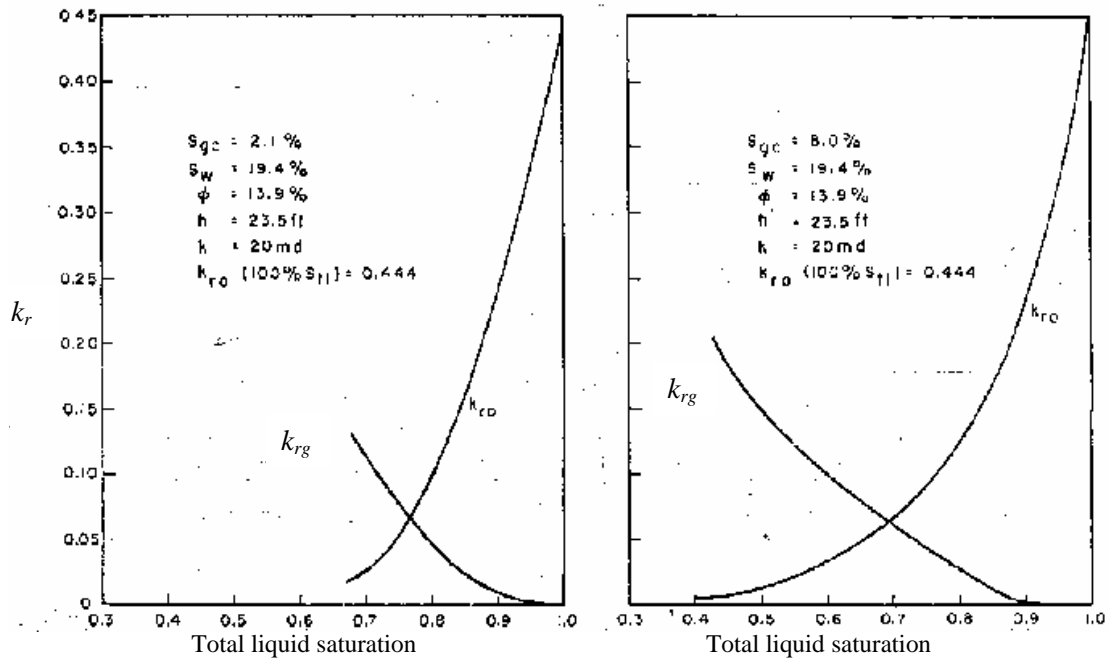


Fig. 12 Relative permeability curves from Vogel's paper¹

Neural Network Models

After finishing the simulation runs and generating the IPR curves, I arranged all the data from the simulator results to build the neural network model.

For the learning process for the neural network, I chose input and output parameters. An IPR curve requires only the values of the bottomhole pressure and the corresponding oil flow rate, but defining a specific IPR curve requires more parameters. These input parameters should have a relationship with the output.

I designed three neural networks with Vogel's input and output parameters, arranging the data in different ways to cover all the possibilities for neural network to find the best solution.

First Model. In the first model I tried to build a neural network model that could predict the oil flow rate by including all the parameters that have direct or indirect effect on the flow rate. The data were taken directly from the simulator model without any preprocessing except for the oil flow rate, which was obtained by interpolation.

I considered the following as inputs for the input layer,

- 1- The recovery factor, N_p/N .
- 2- Flowing bottomhole pressure, p_{wf} .
- 3- Average reservoir pressure, p_r .
- 4- Maximum oil flow rate, $q_{o\max}$.
- 5- Bubblepoint pressure, p_b .

- 6- Oil formation volume factor at bubblepoint pressure, B_{ob} .
- 7- Oil viscosity at bubblepoint pressure, μ_{ob} .
- 8- Solution gas-oil ratio at bubblepoint pressure, R_{sb} .
- 9- Gas formation volume factor at bubblepoint pressure, B_{gb} .
- 10- Gas viscosity at bubblepoint pressure, μ_{gb} .
- 11- Critical gas saturation, S_{gc} .

The output is the oil flow rate, q_o .

I considered the oil and gas properties at bubblepoint because it is difficult to have the oil and gas properties at each pressure, but the properties at the bubblepoint will be fixed for the whole life of the reservoir.

For building the neural network model I used *STATISTICA Neural Networks* software, which includes an option called Intelligent Problem Solver (IPS). This option allows the software to test many neural network architectures and select the best networks. The user has to specify how many networks need to be retrieved from the tested networks.

I determined which network works better for the data set, I left the IPS to test the entire library of available network types, and then I retrieved the best networks. IPS tested the Linear Network, Generalized Regression Neural Network (GRNN), the Probabilistic Neural Network (PNN), the Radial Basis Function (RBF) Network, and the Multilayer Perceptron (MLP) Network with one and two hidden layers. The best networks were the MLP with one and two hidden layers; therefore, all the remaining work was performed only on the MLP.

After training was completed, the software tested different MLP architectures by changing the number of hidden layers, one or two, and the number of nodes in the hidden layers. The best network found was the one with five input nodes (N_p/N , p_{wf} , $q_{o\max}$, p_r , and μ_{gb}), five hidden nodes, and one output node (**Fig. 13**). Weights and thresholds for the network are tabulated in **Tables 4** and **5**. This network found that these five input parameters affected the q_o .

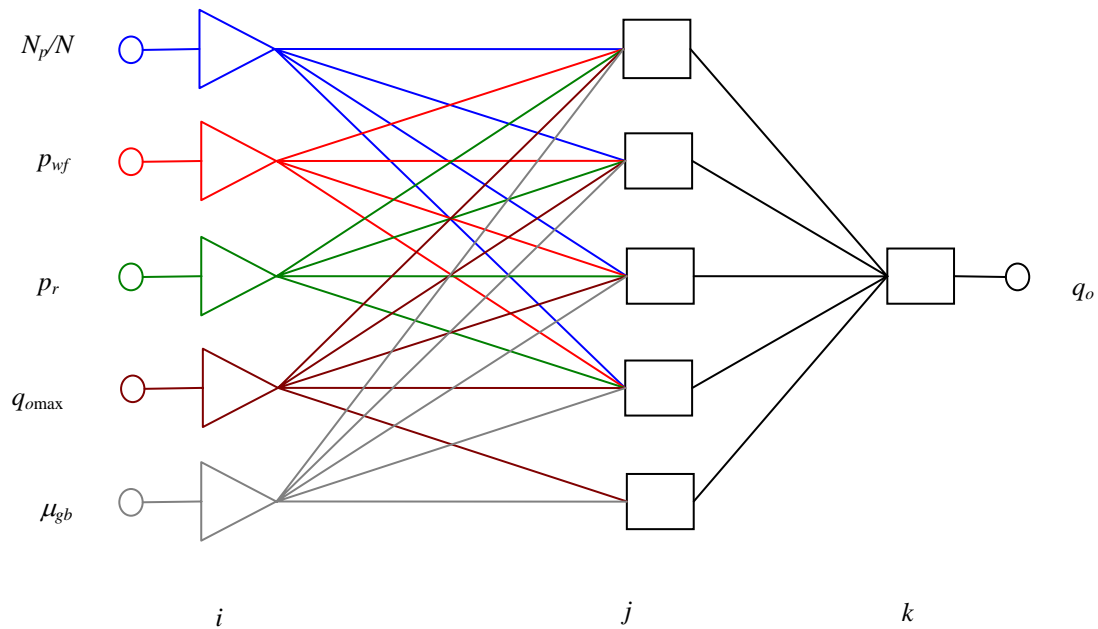


Fig. 13 Illustration for the construction of the first neural network model

Table 4 - The weights for first neural network model						
		<i>J</i>				
		1	2	3	4	5
<i>i</i>	1	0.095694	0.28260	-0.118643	0.173360	-0.115229
	2	-0.316322	-2.24489	0.657257	0.844103	-0.972225
	3	0.105862	1.14525	0.133993	0.345051	-0.312361
	4	0.730777	-0.18464	1.293967	-0.930935	1.079821
	5	-0.047286	0.19473	-0.078116	0.152635	0.007135
<i>k</i>	1	0.83540	2.31298	1.51986	-1.36656	1.49853

Table 5 - Threshold for first neural network model					
<i>J</i>					<i>k</i>
1	2	3	4	5	1
0.642428	-1.39777	0.009031	-0.779553	1.053500	1.20079

Activation function for the hidden layer is the hyperbolic function

$$f(x) = \frac{e^x - e^{-x}}{e^x + e^{-x}}, \dots\dots\dots (6)$$

and the activation function for the output layer is the logistic function

$$f(x) = \frac{1}{1 + e^{-x}}, \dots\dots\dots (7)$$

Second Model. Although the neural network solved a complex relationship that could not be solved by traditional mathematical methods, it is desirable to simplify the relationship for better performance.

For simplifying the relationship, I tried to build a neural network that can establish the relationship between the $q_o/q_{o\max}$ and p_{wf}/p_r . In the first model, the plot of q_o

versus p_{wf} shows different curves with a wide range of q_o values. In our case, all the curves are similar and follow the same trend.

I considered the following as inputs:

- 1- The recovery factor, N_p/N .
- 2- Dimensionless pressure, p_{wf}/p_r .
- 3- Bubblepoint pressure, p_b .
- 4- Oil formation volume factor at bubblepoint pressure, B_{ob} .
- 5- Oil viscosity at bubblepoint pressure, μ_{ob} .
- 6- Solution-gas-oil ratio at bubblepoint pressure, R_{sb} .
- 7- Gas formation volume factor at bubblepoint pressure, B_{gb} .
- 8- Gas viscosity at bubblepoint pressure, μ_{gb} .
- 9- Critical gas saturation, S_{gc} .

The output is the dimensionless oil flow rate, $q_o/q_{o\max}$.

The value of $q_o/q_{o\max}$ is always between 0 and 1. So, when the neural network model is used to predict future values of $q_o/q_{o\max}$, the predicted values must fall between 0 and 1, which makes the job of the neural network model easier by setting a range for the predicted values.

With using the IPS, the best network was the MLP. The best architecture was for three input nodes (μ_{gb} , B_{ob} , and p_{wf}/p_r), using three hidden nodes, and one output node (**Fig. 14**). Weights and thresholds for the network are tabulated in **Tables 6** and **7**.

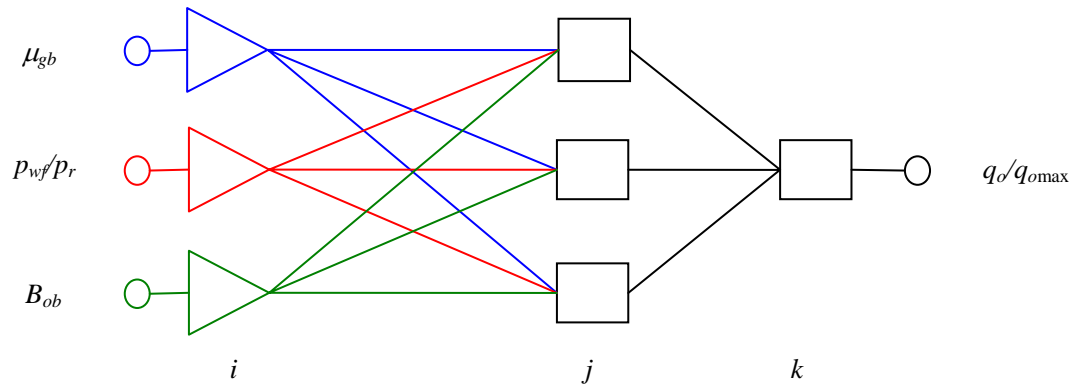


Fig. 14 Illustration for the construction of the second neural network model

		<i>j</i>		
		1	2	3
<i>i</i>	1	-1.19333	-2.62913	-1.40054
	2	-0.13539	0.18450	-0.08751
	3	-0.26119	0.18477	-0.04386
<i>k</i>	1	1.478838	3.418597	1.560448

<i>j</i>			<i>k</i>
1	2	3	1
-0.10841	-2.90354	0.09337	0.837178

Activation function for the hidden layer is the hyperbolic function (**Eq. 6**), and the activation function for the output layer is the logistic function (**Eq. 7**).

Third Model. In the Vogel¹ and Fetkovich⁶ equations, the average reservoir pressure p_r is considered as an input to establish the IPR curve. This model considers p_r as an output.

I considered the following as inputs:

- 1- The recovery factor, N_p/N .
- 2- Flowing bottomhole pressure, p_{wf} .
- 3- Maximum oil flow rate, q_{omax} .
- 4- Bubblepoint pressure, p_b .
- 5- Oil formation volume factor at bubblepoint pressure, B_{ob} .
- 6- Oil viscosity at bubblepoint pressure, μ_{ob} .
- 7- Solution gas-oil ratio at bubblepoint pressure, R_{sb} .
- 8- Gas formation volume factor at bubblepoint pressure, B_{gb} .
- 9- Gas viscosity at bubblepoint pressure, μ_{gb} .
- 10- Critical gas saturation, S_{gc} .

The outputs are the oil flow rate, q_o , and the average reservoir pressure, p_r .

As the oil is produced, the oil in place decreases and in consequence the average reservoir pressure decreases. In this model I am trying to determine whether the neural network can predict the relationship between the cumulative oil produced and the average reservoir pressure.

The learning process was performed with only the MLP. From the best five models, I selected the one with five input nodes (N_p/N , p_{wf} , q_{omax} , R_{sb} , and B_{ob}), five

hidden nodes, and two output nodes (**Fig. 15**). Weights and thresholds for the network are tabulated in **Tables 8** and **9**.

The activation function for the hidden layer is hyperbolic (**Eq. 6**), and logistic for the output layer (**Eq. 7**).

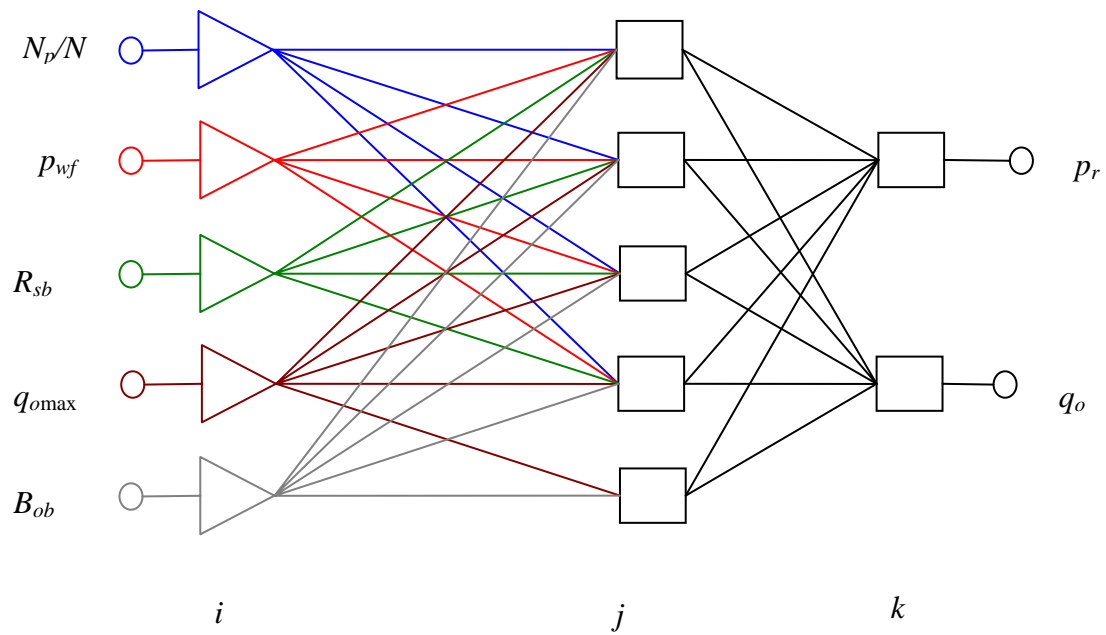


Fig. 15 Illustration for the construction of the third neural network model

Table 8 - The weights for third neural network model						
		<i>j</i>				
		1	2	3	4	5
<i>i</i>	1	0.810700	0.055842	-0.173058	0.63933	-0.006894
	2	0.247285	1.313917	1.365727	-0.14048	-0.204629
	3	-0.206950	-0.349037	0.624382	-1.00049	0.300263
	4	0.534303	0.120481	0.162954	-0.00439	-0.371571
	5	0.208213	-0.144539	-0.061151	-0.47161	0.284447
<i>k</i>	1	0.21009	-1.26307	1.18380	0.30444	0.31154
	2	-0.227246	0.006402	-0.036087	-0.818592	0.091393

Table 9 - Threshold for third neural network model						
<i>j</i>					<i>k</i>	
1	2	3	4	5	1	2
-0.633504	0.232344	0.158766	0.03563	0.577545	0.02651	-0.522668

MODEL EVALUATION AND DISCUSSION

To test the accuracy of prediction of each of the three neural network models, I introduced new data that were not used in the training process. The predicted values differ from the actual values, and to evaluate the accuracy of the models, I used the percentage relative error

$$\text{Percentage Relative Error (e}_r\text{ (\%))} = \left(\frac{\text{Predicted value} - \text{Actual value}}{\text{Actual value}} \right) \times 100 \quad \dots\dots\dots (8)$$

It gives an indication of the relative deviation of the predicted data from the actual data. Number of data points used for training is 1208 data points, and for evaluation is 50 data points.

The first and the second models were compared to results generated using Vogel's equation,

$$\frac{q_o}{q_{o\max}} = 1 - 0.2 \frac{p_{wf}}{p_r} - 0.8 \left(\frac{p_{wf}}{p_r} \right)^2, \quad \dots\dots\dots (2)$$

For establishing the dimensionless IPR curve using Vogel's equation we need to have either p_{wf} and p_r , or q_o and $q_{o\max}$. On the other hand, if we want to establish the IPR curve, we need to have any three of the four parameters in the equation.

I can only compare the first and the second model to Vogel's equation, but not the third model. The input parameters used in the third model to establish an IPR curve are not enough to establish an IPR curve using Vogel's equation.

First Model. The percentage relative error for 80% of the training data is between 15% and -15% (**Fig. 16**), which indicates high accuracy for the model prediction. The same results were obtained for the evaluation data (**Fig. 17**).

Fig. 18 shows percentage relative error for predicted q_o using Vogel's equation, where 71% of the predictions have percentage relative error between -15% and 15%. The first model shows higher accuracy than Vogel's equation.

Fig. 17 shows the percentage relative error of the evaluation data for both first model and Vogel's equation. In this figure, Vogel's equation has better performance than the first model. The percentage relative error is between -15% and 15% for 94% of the data resulted from Vogel's equation and for 79% of the data resulted from the first model.

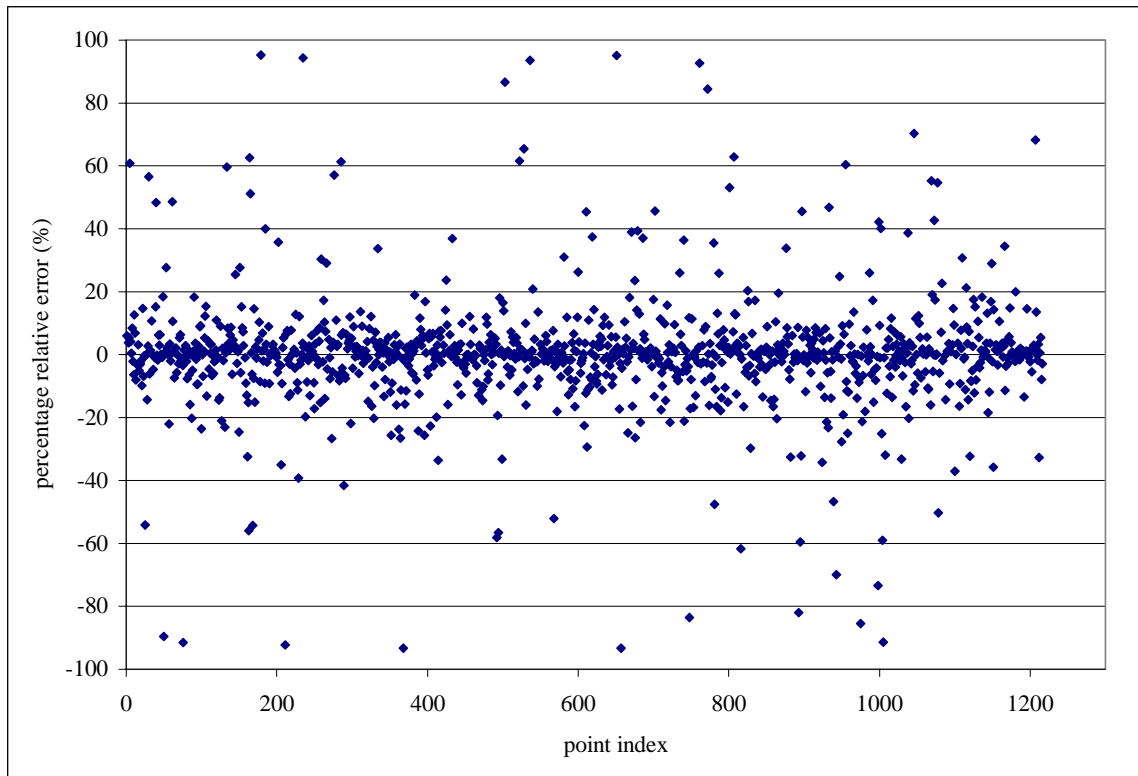


Fig. 16 Percentage relative error of the predicted q_o for training data (first model)

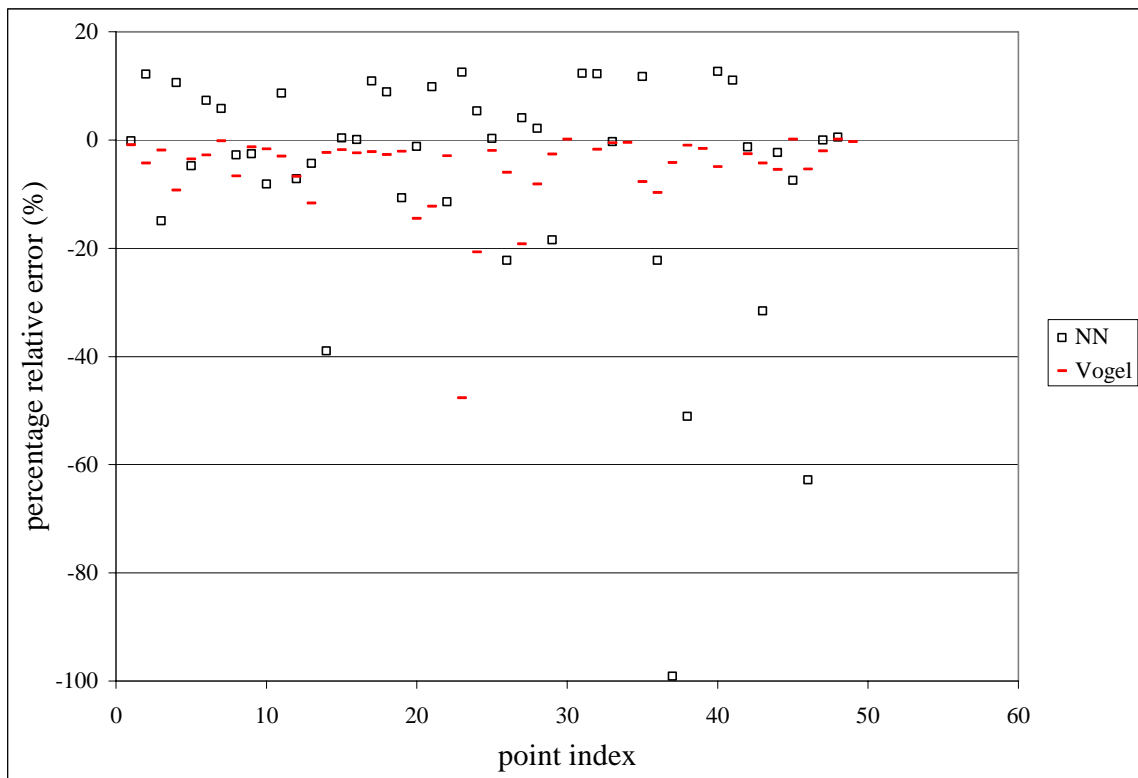


Fig. 17 Percentage relative error of the predicted q_o for evaluation data (first model versus Vogel's equation)

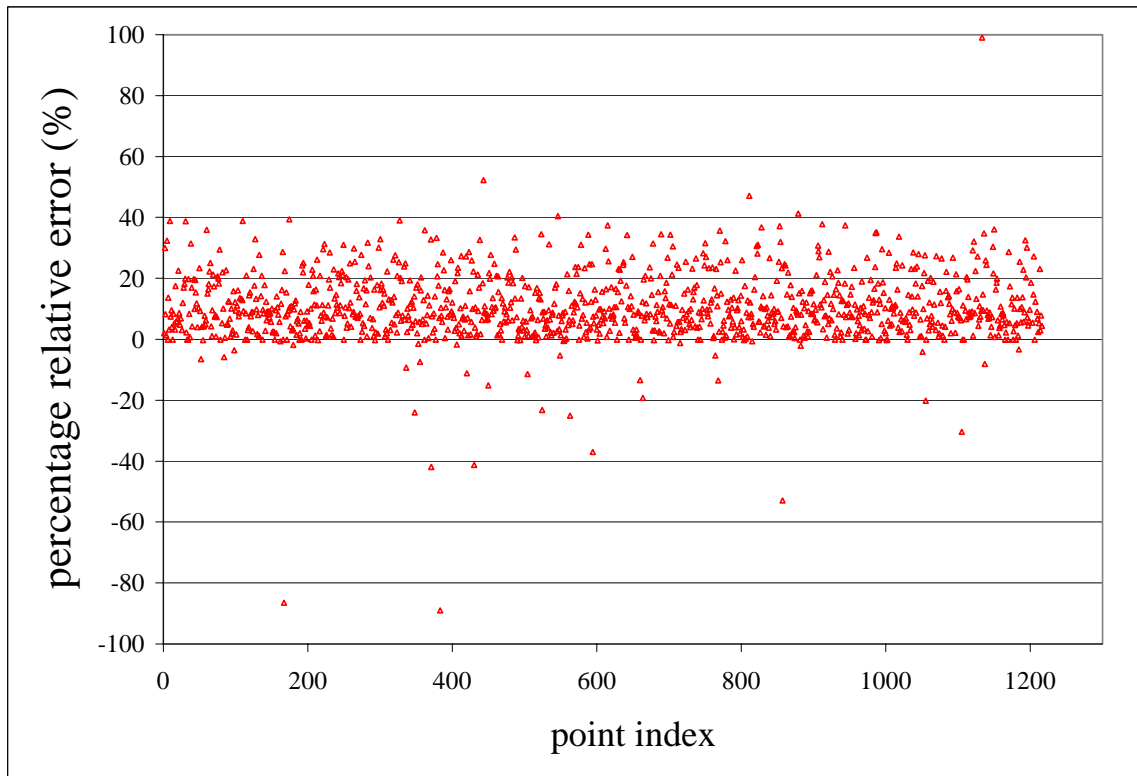


Fig. 18 Percentage relative error of the predicted q_o for training data (Vogel's equation)

The first model has the same error range for almost the same percentage amount of the data for both training and evaluation data. Vogel's equation has for the same error range a significant difference in the percentage amount of the data for training and evaluation data.

Fig. 19 shows selected three IPR curves from the training data. The first model is better than Vogel's equation for two IPR curves.

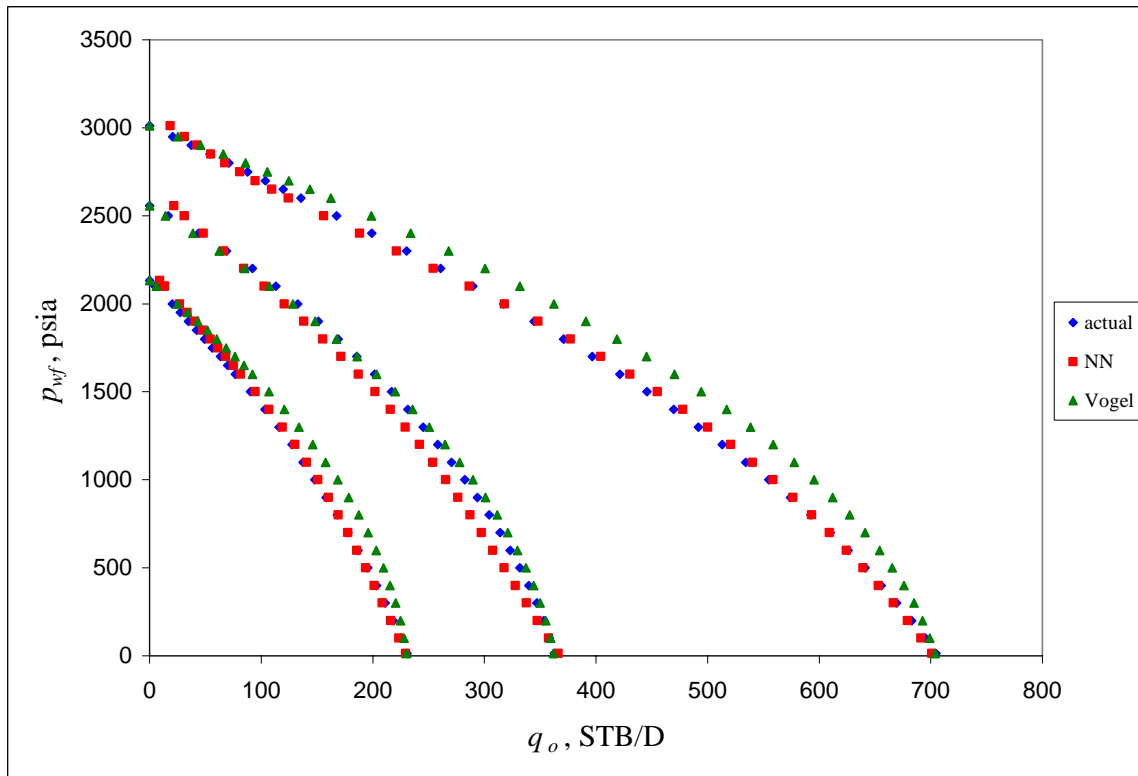


Fig. 19 Comparing the IPR curves produced using the first model and Vogel's equation to the actual IPR curves

Fig. 20 shows a crossplot for the training data comparing the predicted data with the actual data, which reflects good prediction by the first model. If a point lies on a 45° line, that means the predicted point equals exactly the actual point.

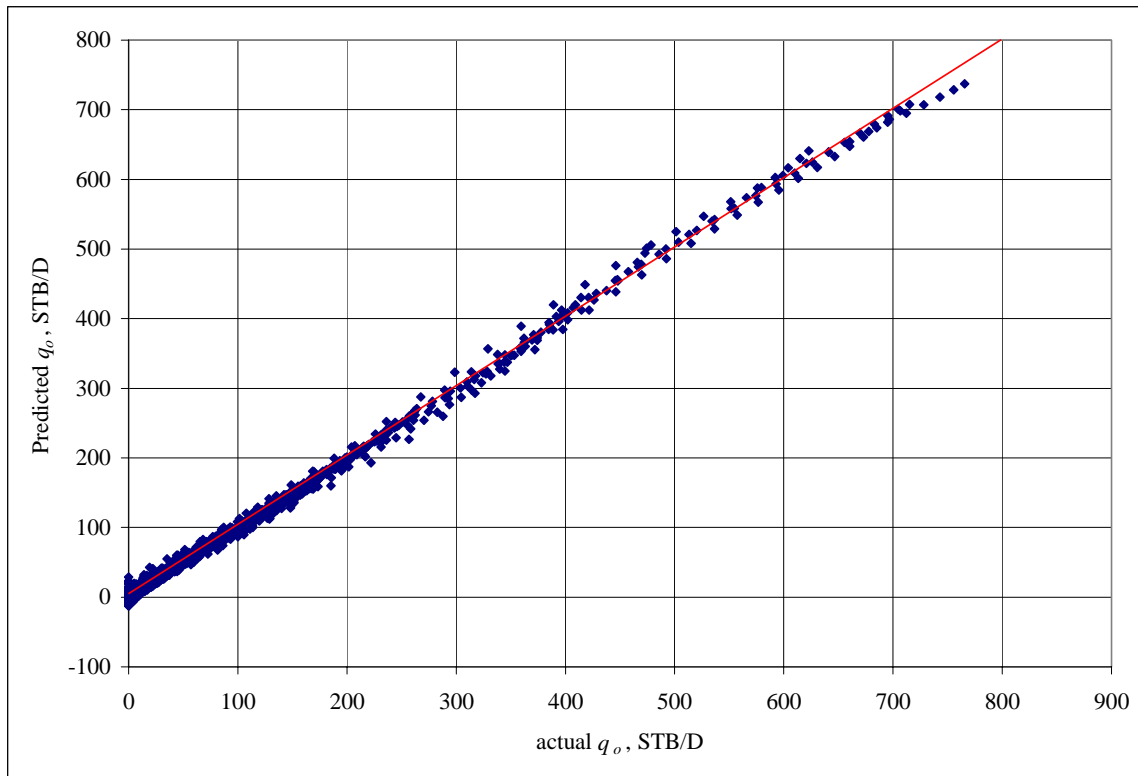


Fig. 20 Crossplot for q_o for training data (first model)

Second Model. The model predicts $q_o/q_{o\max}$. **Fig. 21** compares the second model and Vogel's equation to simulation results. Vogel's equation is overestimating the actual values, where the second model is overlaying the simulation values. The percentage relative error for about 90% of the training data is between 10% and -10% (**Fig. 22**), which gives very good indication for the high accuracy of the model in prediction. Where for the evaluation data, the results show slightly lower accuracy than the training data. The percentage relative error is between 10% and -10% for 85% of the data. (**Fig. 23**).

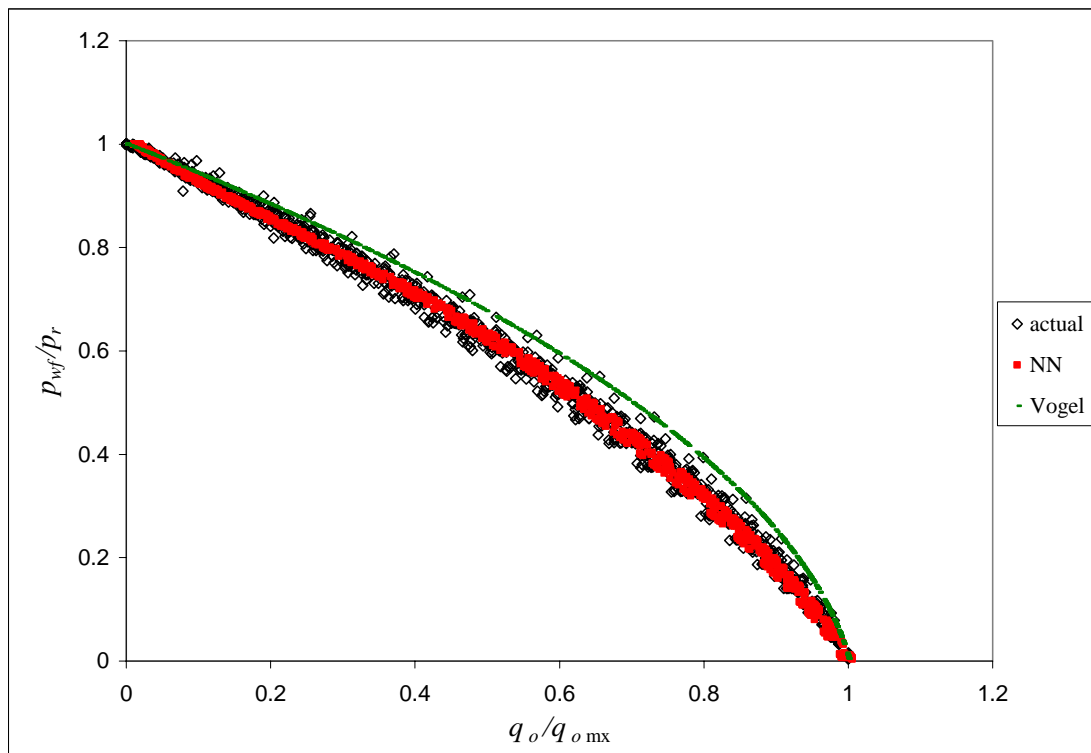


Fig. 21 Dimensionless IPR for actual, second model, and Vogel's equation

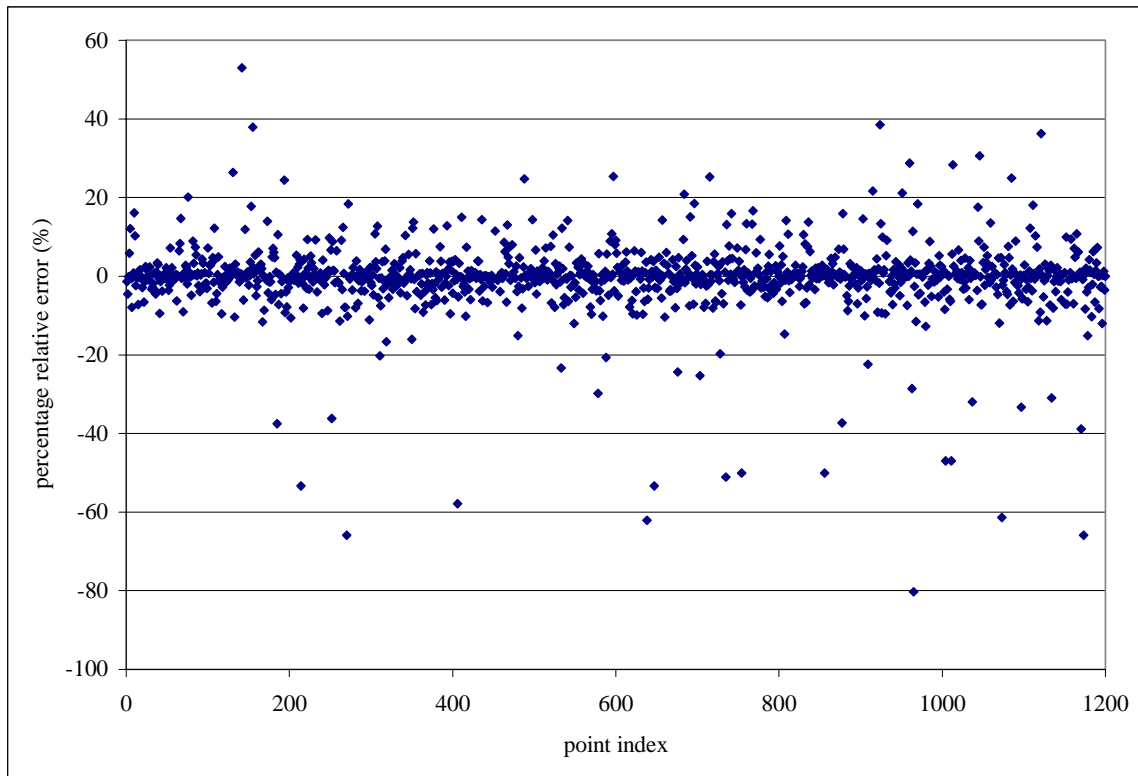


Fig. 22 Percentage relative error of the predicted $q_o/q_{o\max}$ for training data (second model)

The second model predicted outputs with higher accuracy than the first model and the range of the error for training and evaluation data was almost the same for the same percentage amount of the data.

The percentage relative error when Vogel's equation used was between -10% and 10% for about 55% of the training data (**Fig. 23**) and 87% for the evaluation data (**Fig. 24**). As in the first model case, for Vogel's equation for the same error range we have significant difference between the percentage amount of the data for the training and the evaluation data.

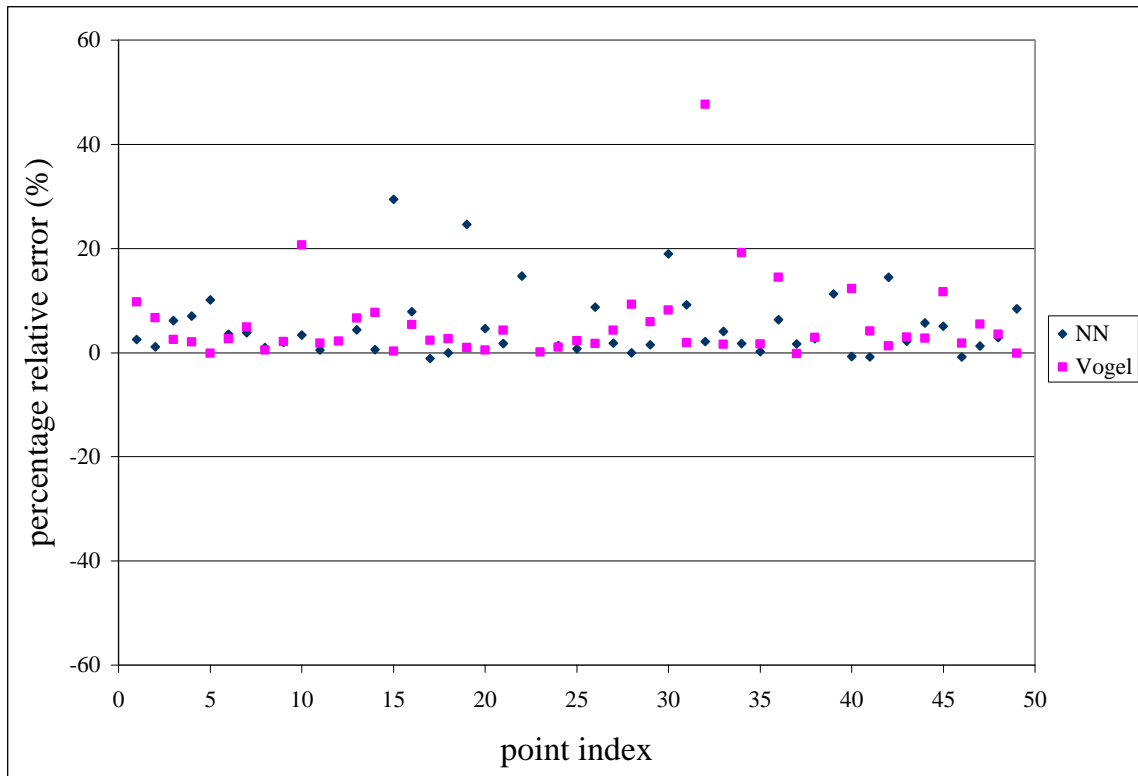


Fig. 23 Percentage relative error of the predicted $q_o/q_{o\max}$ for evaluation data (second model versus Vogel's equation)

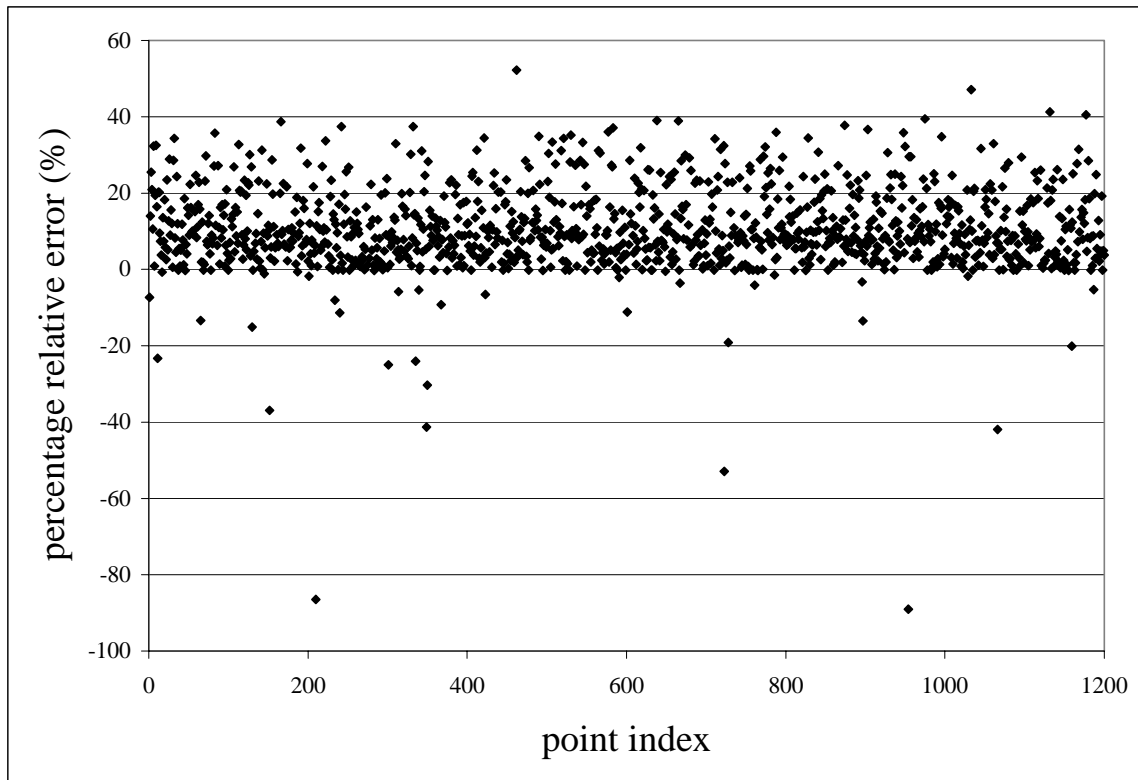


Fig. 24 Percentage relative error of the predicted $q_o/q_{o\max}$ for training data (Vogel's equation)

The results show very good model predictions for both the training and evaluation data, and it can be observed in the crossplot in **Fig. 25** which shows very good agreement for the predicted values with the actual values.

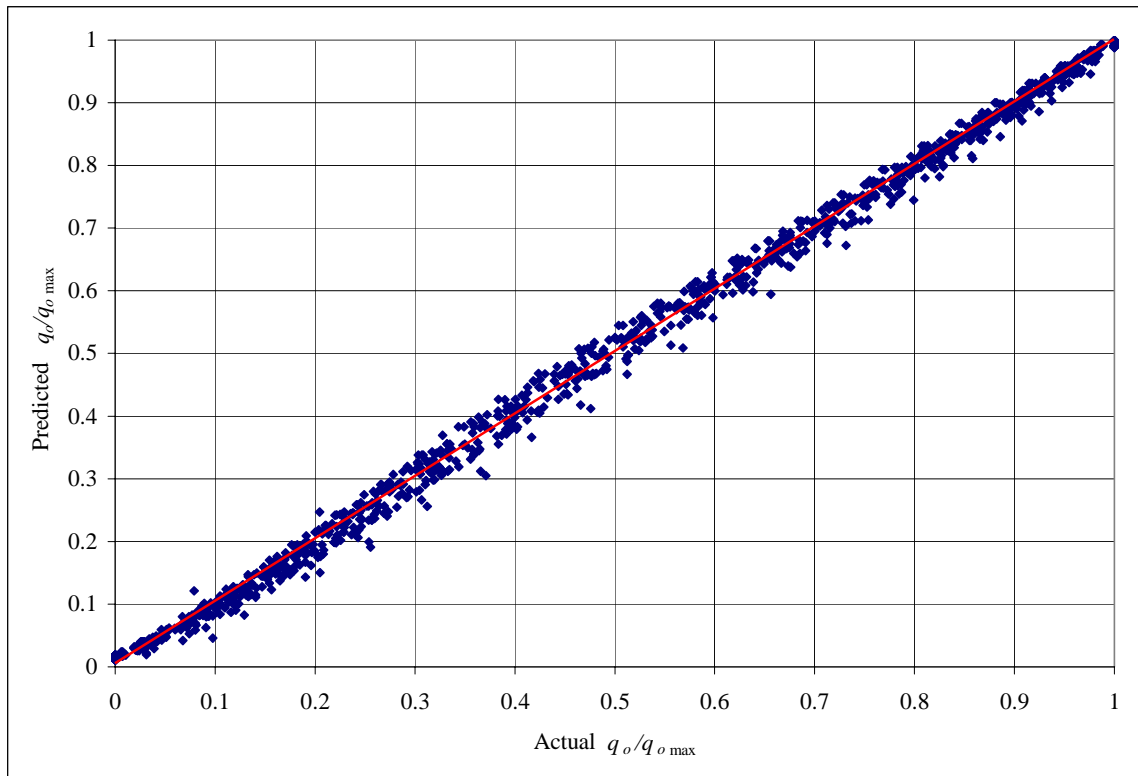


Fig. 25 Crossplot for $q_o/q_{o\max}$ for training data (second model)

Third Model. This model showed moderate error. This model is more complicated than the previous two. I am trying to predict with this model two parameters with different natures. For a single IPR curve, q_o is always changing with changing p_{wf} . On the contrary, I have only one value for p_r .

For the training data, the percentage relative error for q_o was between -20% and 20% for about 70% of the data (**Fig. 26**), and for p_r , it was between -10% and 10% for about 88% of the data (**Fig. 27**).

For the evaluation data, the percentage relative error was the same for q_o (**Fig. 28**), and for p_r , it was divided into two groups. The first group has 26% of the data and the percentage relative error is between 15% and 25%. The second group has 74% of the data and percentage error is between -10% and 0% (**Fig. 29**).

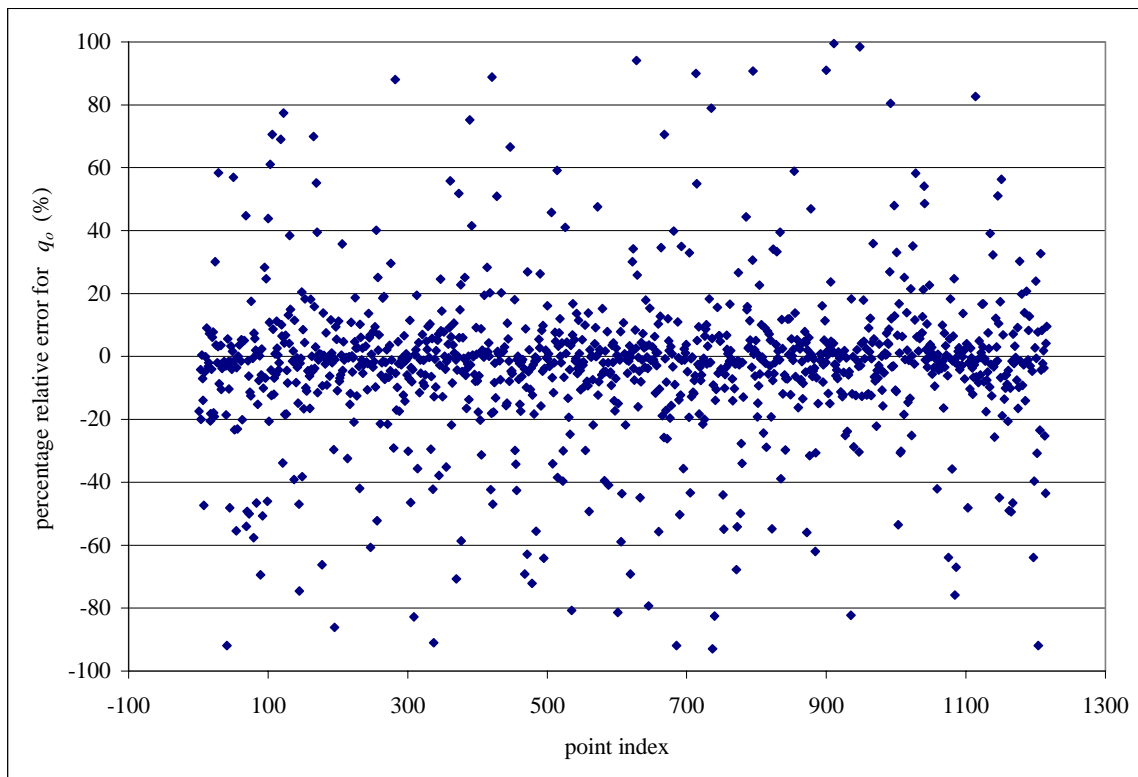


Fig. 26 Percentage relative error of the predicted q_o for training data (third model)

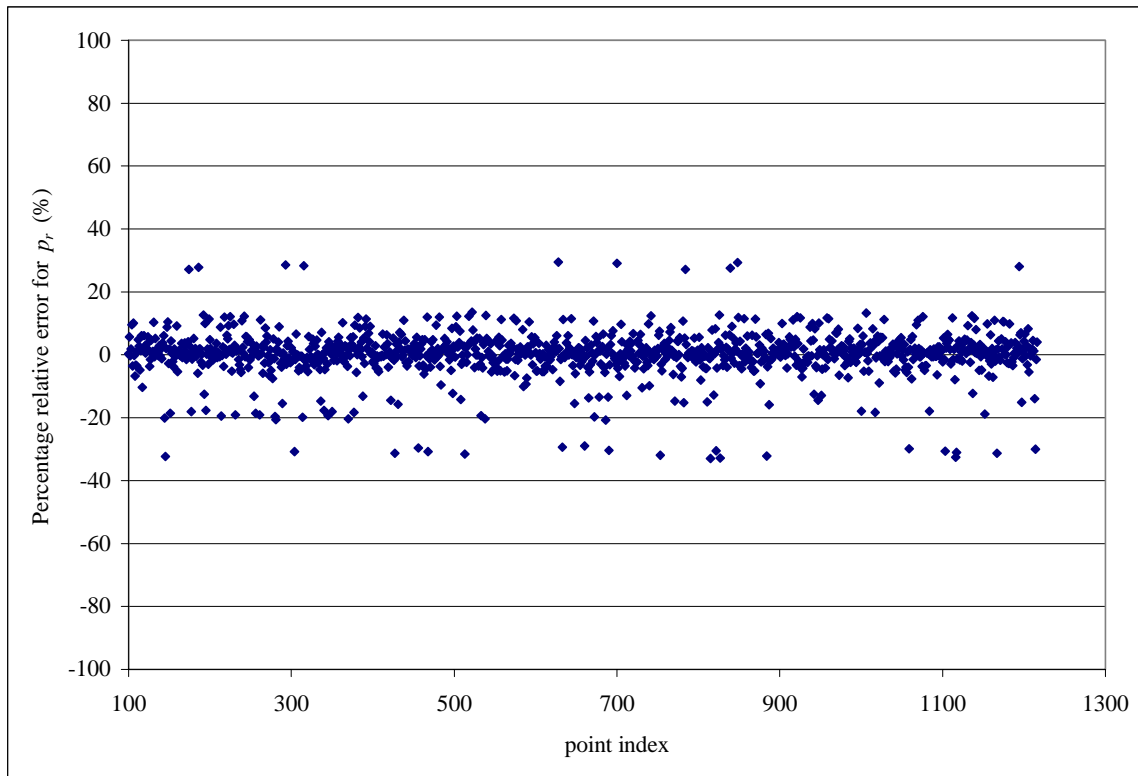


Fig. 27 Percentage relative error of the predicted p_r for training data (third model)

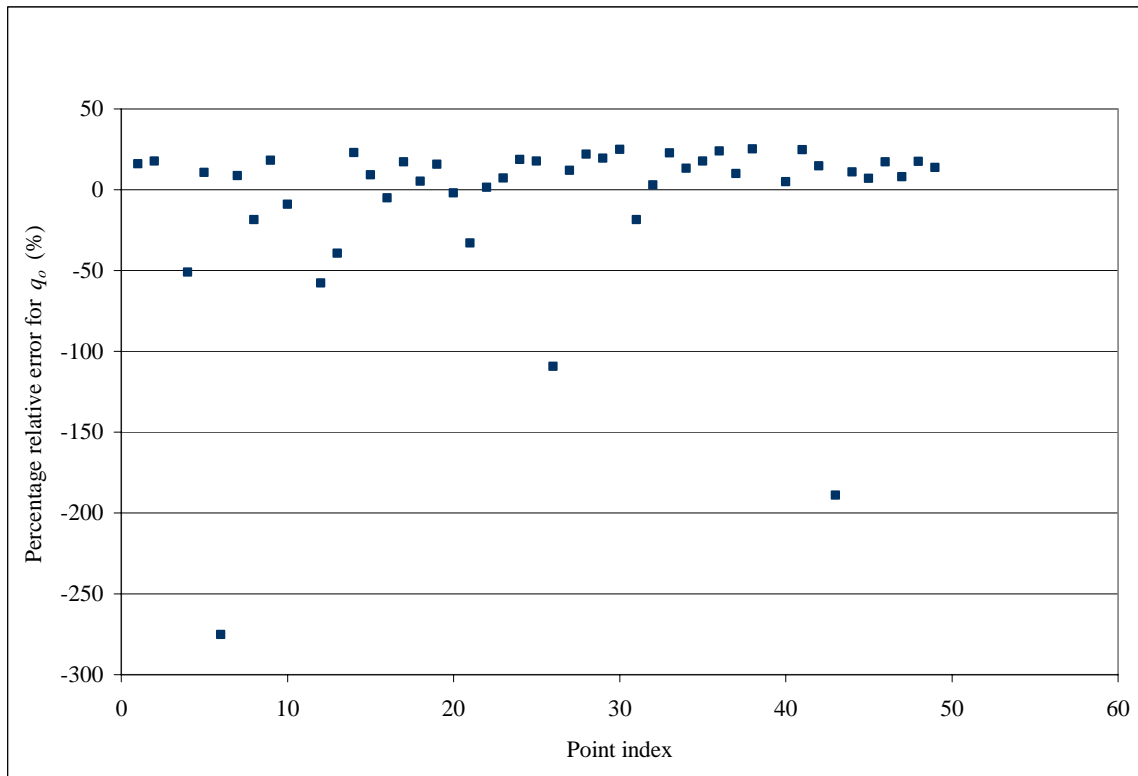


Fig. 28 Percentage relative error of the predicted q_o for evaluation data (third model)

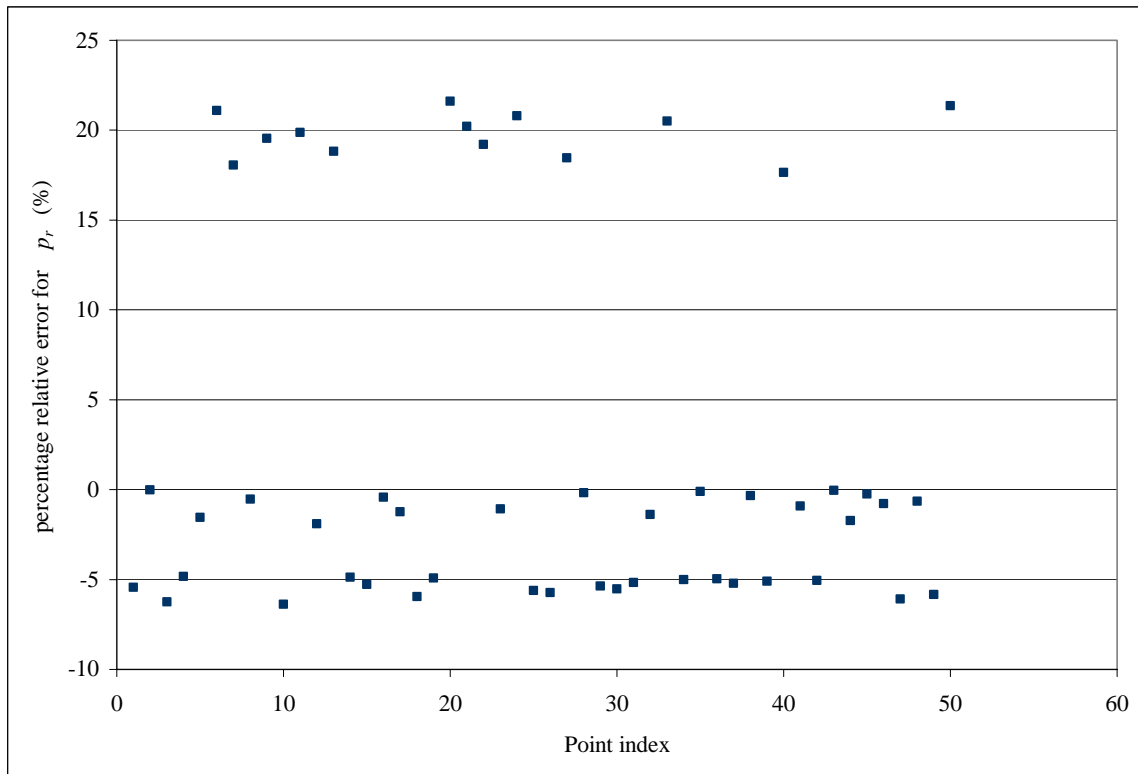


Fig. 29 Percentage relative error of the predicted p_r for evaluation data (third model)

From comparing the results of the predicted and actual data for the training data in the crossplot (**Figs. 30** and **31**), a good agreement can be seen which reflects a good prediction from the neural network model.

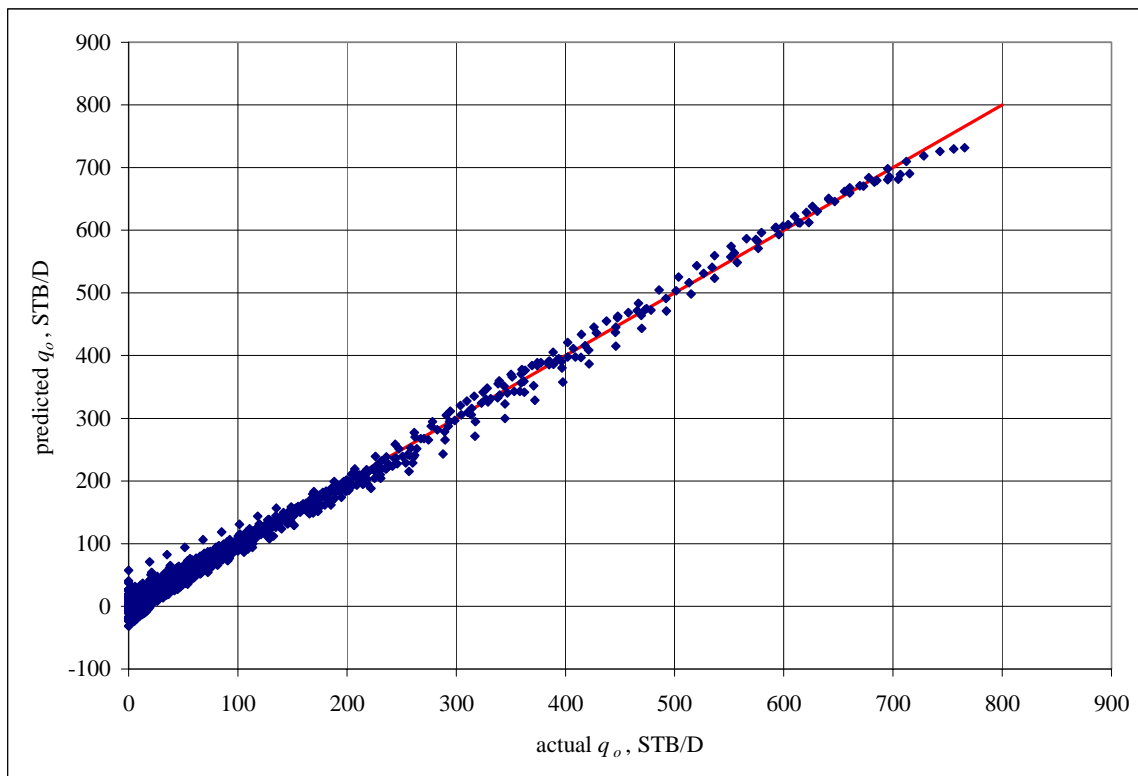


Fig. 30 Crossplot of q_o for training data (third model)

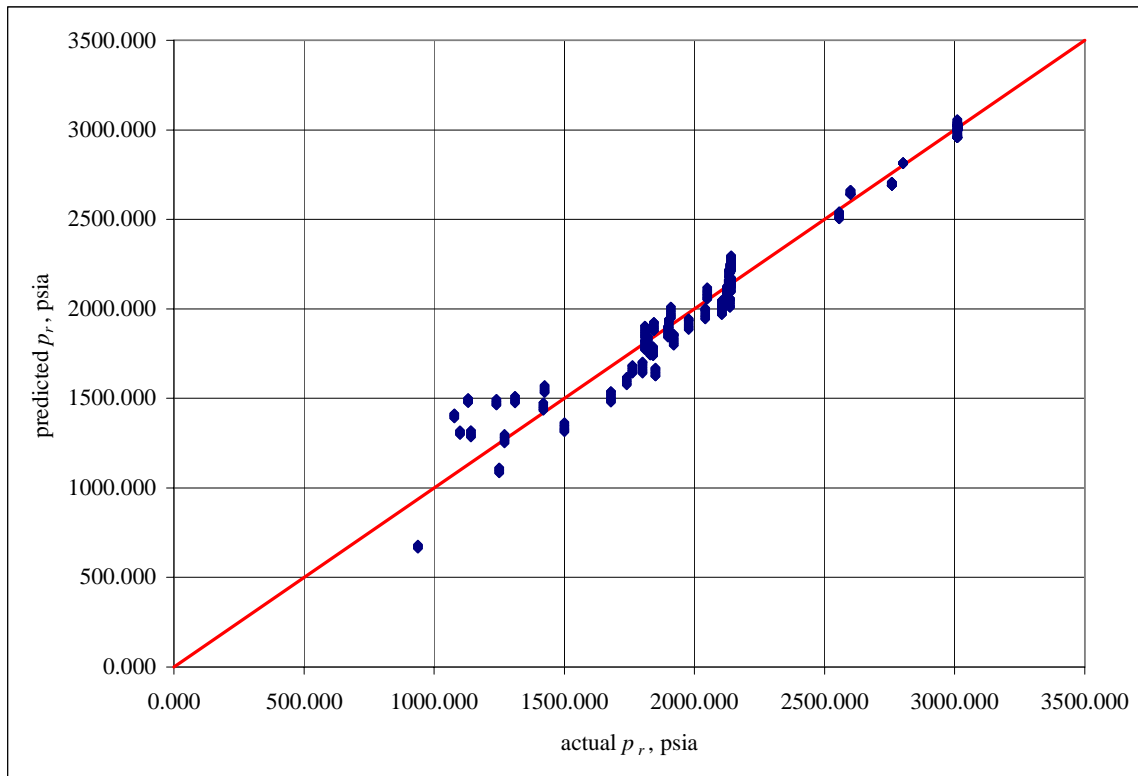


Fig. 31 Crossplot of p_r for training data (third model)

CONCLUSIONS

Three artificial neural networks were developed to establish the inflow performance relationship. The first model predicts the oil flow rate, q_o . The second model predicts the normalized oil flow rate, $q_o/q_{o_{max}}$. The third model predicts the oil flow rate, q_o , and the average reservoir pressure, p_r .

Vogel¹ didn't provide sufficient information to reproduce his work. Part of the data presents unrealistic data that can not occur.

The first two models accurately predicted the required output to establish the inflow performance relationship by considering more than one input.

The first model showed a good prediction, and the error increases at the end points of the curves. The results were compared with Vogel's equation. The first model showed higher accuracy than Vogel's equation for the training data but Vogel's equation produced more accurate results for the evaluation data.

The error was consistent for the first model between the training and the evaluation data but for Vogel's equation, it showed a significant difference.

The second model predicts the output with a higher accuracy than the first model. For the training data the second model showed higher accuracy than Vogel's equation but for the evaluation data it showed similar accuracy to Vogel's equation. Also in this case, the second model showed consistent error for the training and the evaluation data, unlike Vogel's equation that has significant differences between the training and the evaluation data error.

The third model could predict the output with a reasonable accuracy because the two outputs q_o and p_r , have two different natures. If we want to feed one IPR curve to the neural network, we will feed it with different values of q_o but only one value of p_r .

The input data used in the third model to predict q_o and p_r is not enough to be used in Vogel's equation to get the same outputs in the third model.

For establishing the IPR curve using any of the three models, we need to have the $q_{o\max}$ first, which can be calculated from other methods.

This work proved the ability of the neural network to predict the oil flow rate, the dimensionless oil flow rate, and the average reservoir pressure to establish the inflow performance relationship with a good accuracy.

NOMENCLATURE

α	=	timestep increase factor
B_g	=	gas formation volume factor, RB/scf
B_{gb}	=	gas formation volume factor at bubblepoint, RB/scf
B_o	=	oil formation volume factor, RB/STB
B_{ob}	=	oil formation volume factor at bubblepoint, RB/STB
C	=	back-pressure curve coefficient, STB/D/psi ²ⁿ
ϕ	=	porosity, fraction
h	=	formation thickness, ft
J	=	productivity index, STB/D/psi
k	=	absolute permeability, md
k_{ro}	=	oil relative permeability
μ_g	=	gas viscosity, cp
μ_{gb}	=	gas viscosity at bubble point, cp
μ_o	=	oil viscosity, cp
μ_{ob}	=	oil viscosity at bubblepoint, cp
n	=	exponent of back-pressure curve, dimensionless
N	=	initial oil in place
N_p	=	cumulative oil produced, STB
p_b	=	bubblepoint pressure, psia
p_e	=	pressure at the reservoir outer boundary, psia

- p_r = average reservoir pressure, psia
- p_{wf} = flowing bottomhole flowing pressure, psia
- q_o = oil flow rate, STB/D
- $q_{o\max}$ = maximum oil flow rate, STB/D
- r_e = reservoir outer radius, ft
- r_w = wellbore radius, ft
- R_s = solution gas-oil ratio, Mscf/STB
- R_{sb} = solution gas-oil ratio at bubblepoint, Mscf/STB
- S_L = total liquid saturation
- S_{or} = residual oil saturation, fraction
- S_{wc} = irreducible water saturation, fraction

REFERENCES

- 1) Vogel, J.V.: "Inflow Performance Relationship for Solution Gas Drive Wells," *JPT* (1968), 83.
- 2) Weller, W.T.: "Reservoir Performance During Two Phase Flow" *JPT* (February 1966) 240.
- 3) Saputelli, L., Malki, H., Canelon, J. and Nikolaou, M.: "A Critical Overview of Artificial Neural Network Applications in the Context of Continuous Oil Field Optimization," paper SPE 77703 presented at the 2002 SPE Annual Technical Conference and Exhibition, San Antonio, Texas, 29 September – 2 October.
- 4) Shippen, M. E.: "Development of a Neural Network Model for the Prediction of Liquid Holdup in Two-Phase Horizontal Flow" M.S. Thesis, Texas A&M University, College Station (2001).
- 5) Zambrano, G.: "Development of Neural Network Models for the Prediction of Dewpoint Pressure of Retrograde Gases and Saturated Oil Viscosity of Black Oil Systems" M.S. Thesis, Texas A&M University, College Station (2002).
- 6) Evinger, H.H. and Muskat, M.: "Calculation of Theoretical Productivity Factor," *Trans., AIME*, **146** (1942) 126.
- 7) Fetkovich, M. J.: "The Isochronal Testing of Oil Wells" paper SPE 4529 presented at the SPE 48th Fall Meeting Las Vegas, Nevada (1973).
- 8) Standing, M.B.: "Inflow Performance Relationship for Damaged Wells Producing by Solution Gas Drive," *JPT* (November 1970) 1399.
- 9) Brown, K.E.: *Technology of Artificial Lift Methods*, PennWell Publishing Co., Tulsa, Oklahoma (1984) **4**.
- 10) Camacho, R.G. and Raghavan, R.: "Inflow Performance Relationship for Solution Gas Drive Reservoirs" paper SPE 16204 available from SPE, Richardson, Texas (1987).
- 11) Klins, M.A. and Majcher, M. W.: "Inflow Performance Relationship for Damaged or Improved Wells Producing Under Solution-Gas Drive," paper SPE 19852 available from SPE, Richardson, Texas (1992).
- 12) Standing, M.B.: "Concerning the Calculation of Inflow Performance of Wells Producing Solution-Gas Drive Reservoirs" *JPT* (September 1971) 1141.

13) Haykin, S.: *Neural Networks: A Comprehensive Foundation*, second edition, Prentice Hall. Upper Saddle River, New Jersey (1999).

APPENDIX
IPR CURVES GENERATED FROM RESERVOIR SIMULATION

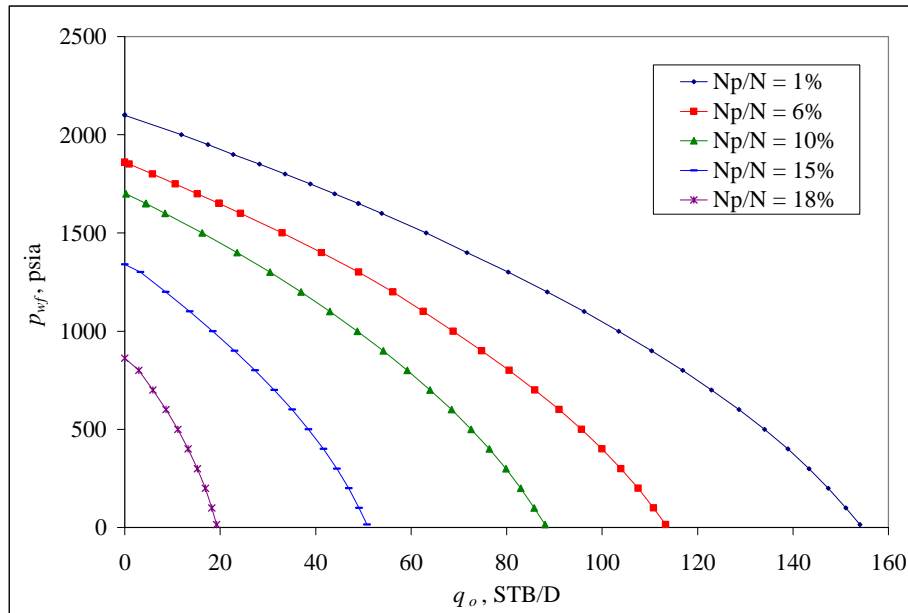


Fig. A-1 IPR curves for case 2 (refer to Table 2)

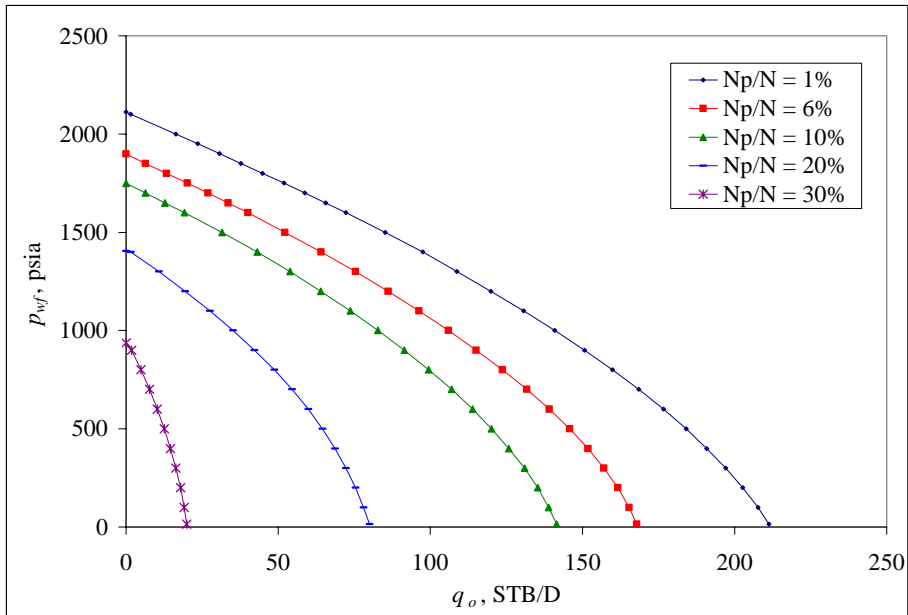


Fig. A-2 IPR curves for case 3 (refer to Table 2)

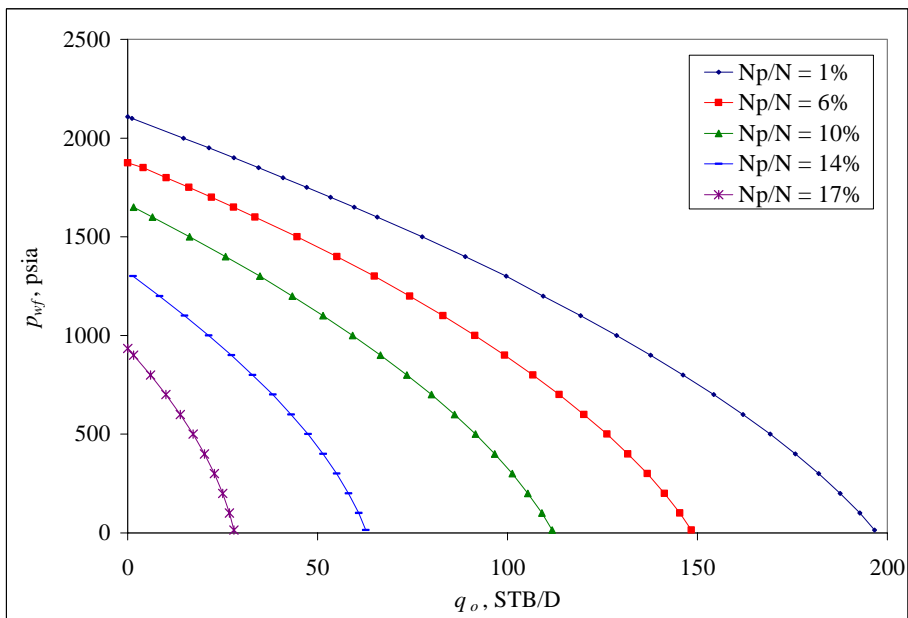


Fig. A-3 IPR curves for case 4 (refer to Table 2)

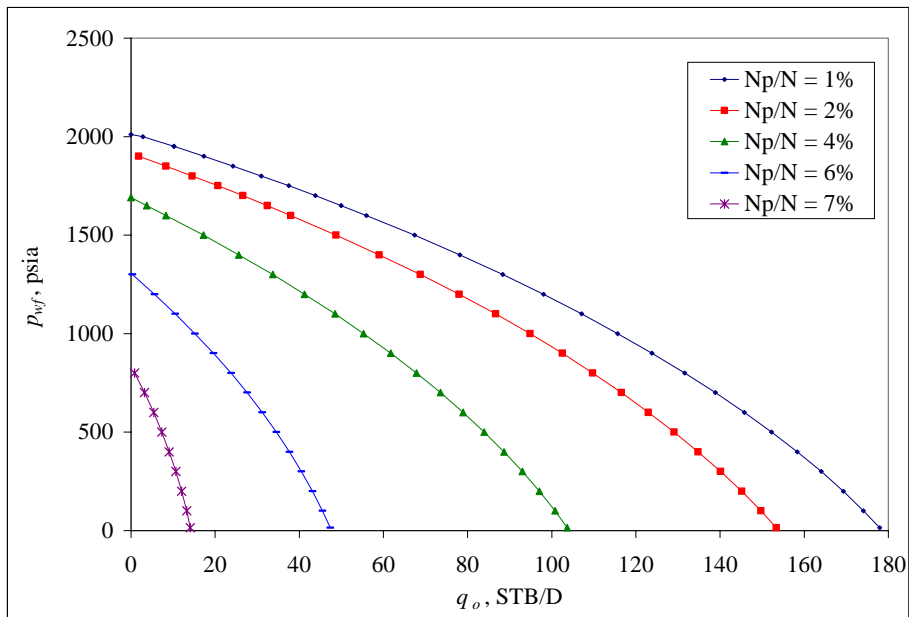


Fig. A-4 IPR curves for case 5 (refer to Table 2)

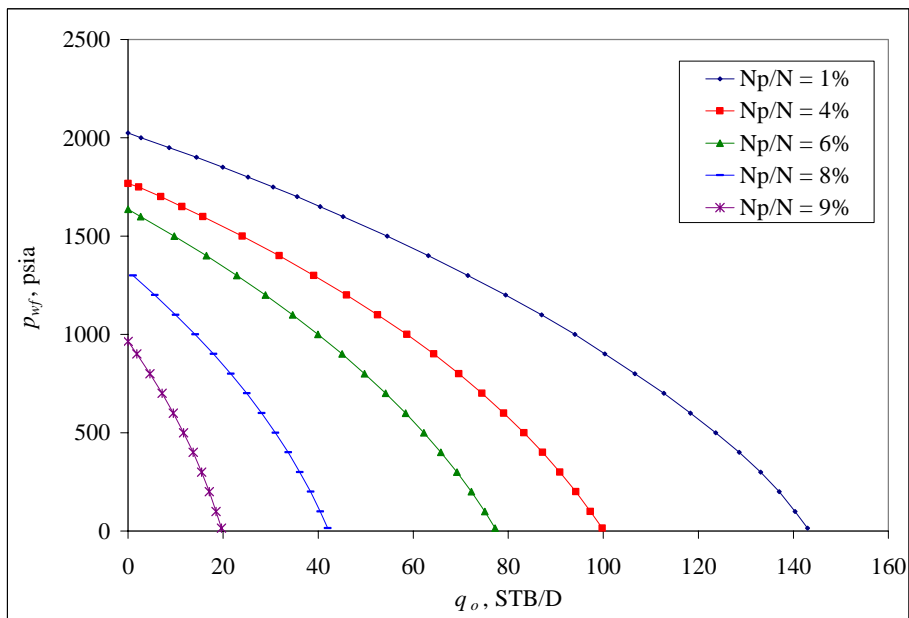


Fig. A-5 IPR curves for case 6 (refer to Table 2)

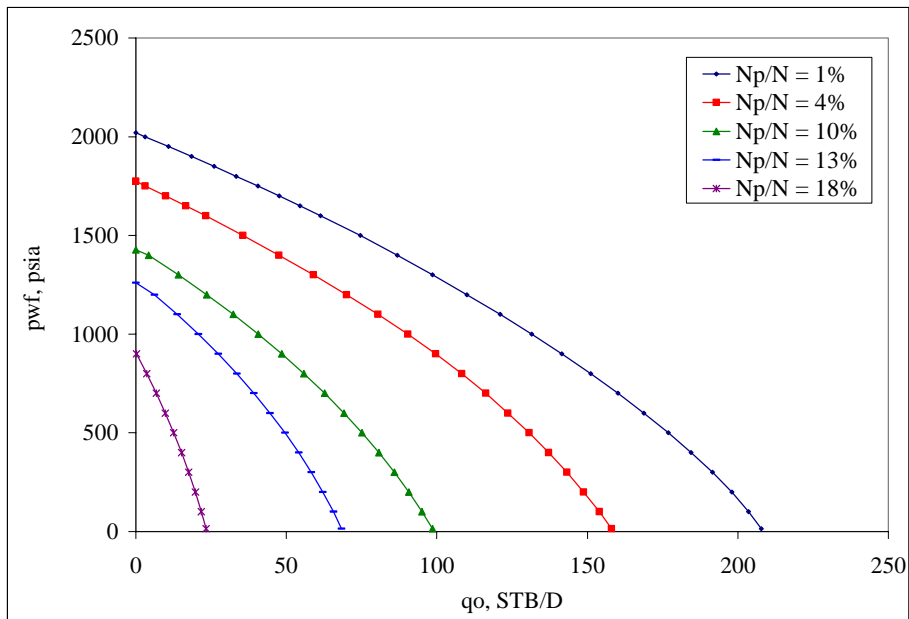


Fig. A-6 IPR curves for case 7 (refer to Table 2)

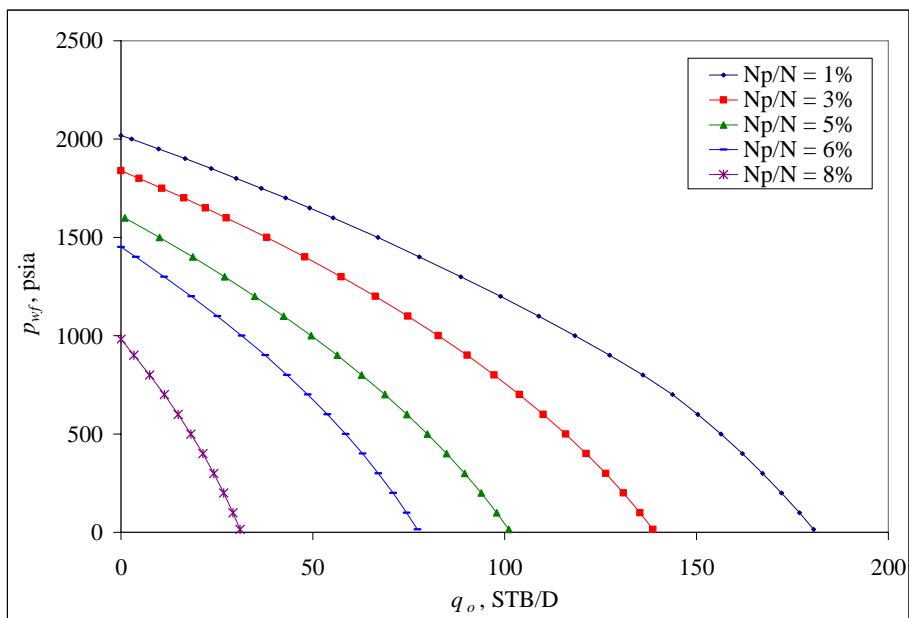


Fig. A-7 IPR curves for case 8 (refer to Table 2)

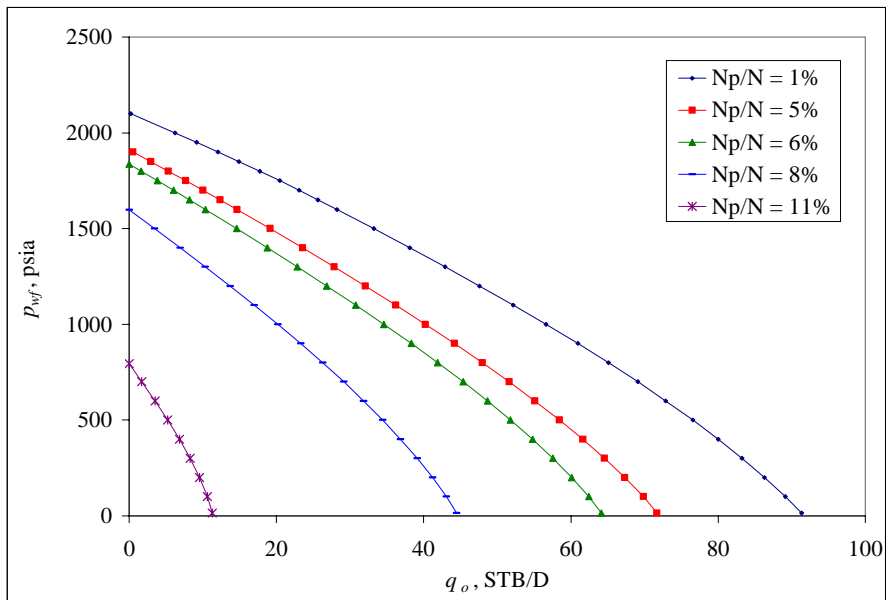


Fig. A-8 IPR curves for case 9 (refer to Table 2)

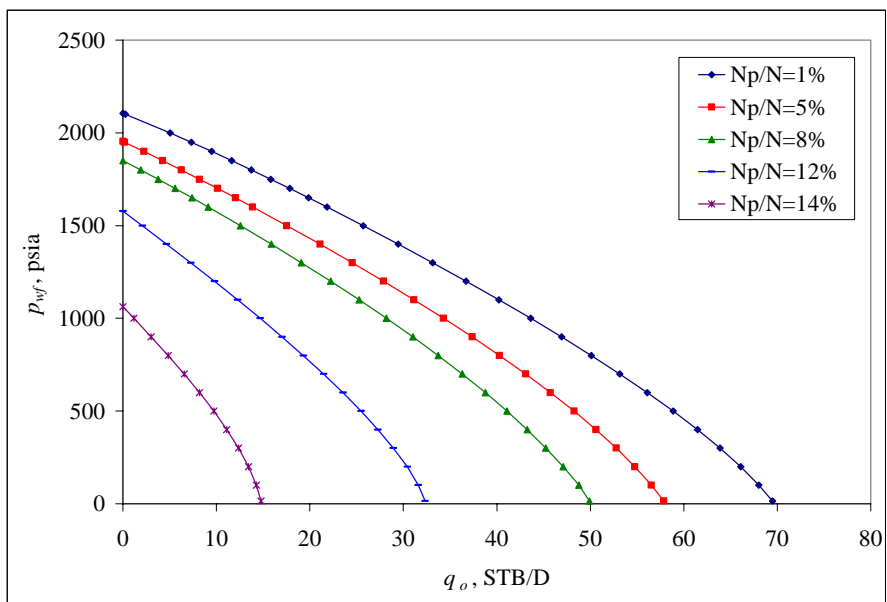


Fig. A-9 IPR curves for case 10 (refer to Table 2)

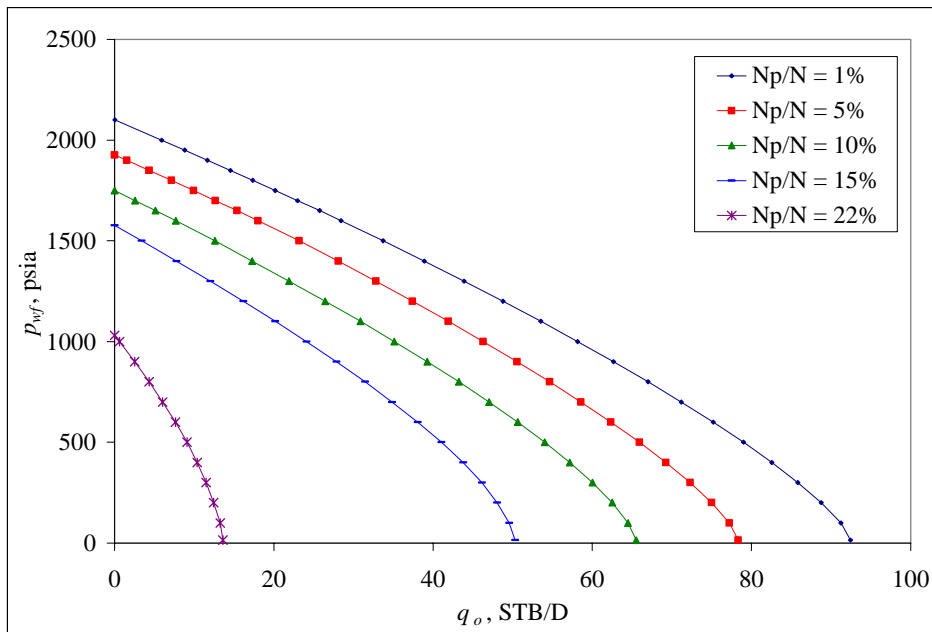


Fig. A-10 IPR curves for case 11 (refer to Table 2)

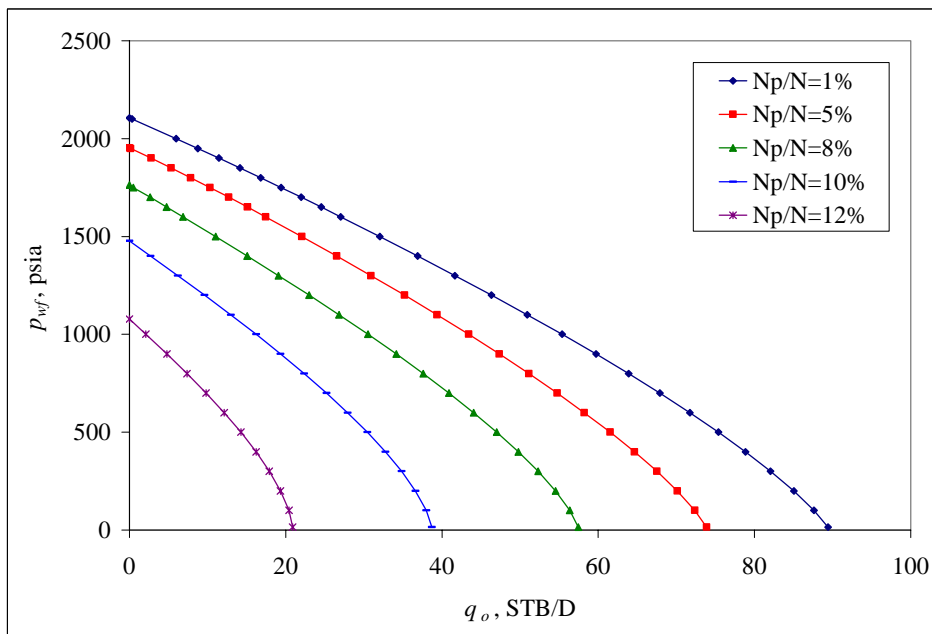


Fig. A-11 IPR curves for case 12 (refer to Table 2)

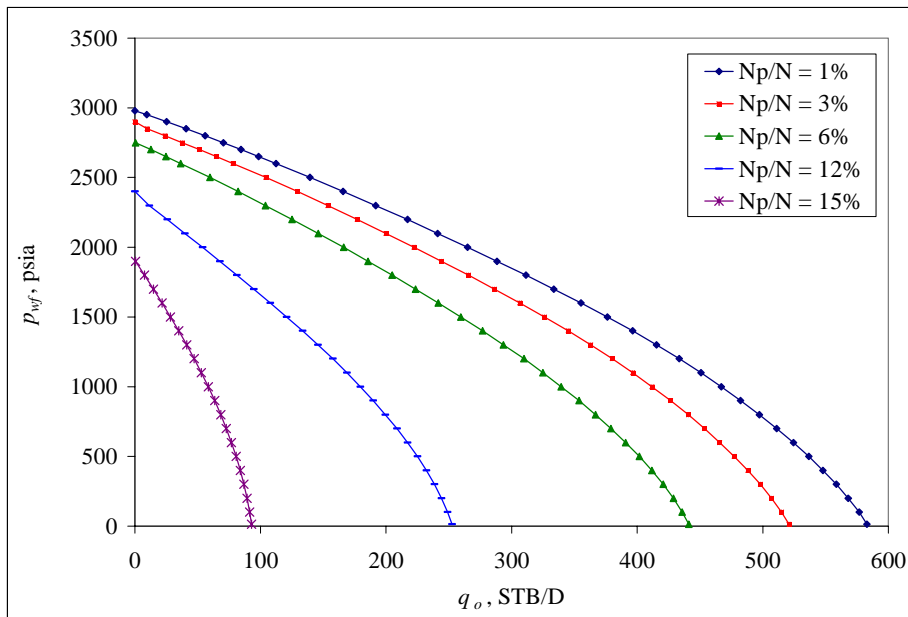


Fig. A-12 IPR curves for case 13 (refer to Table 2)

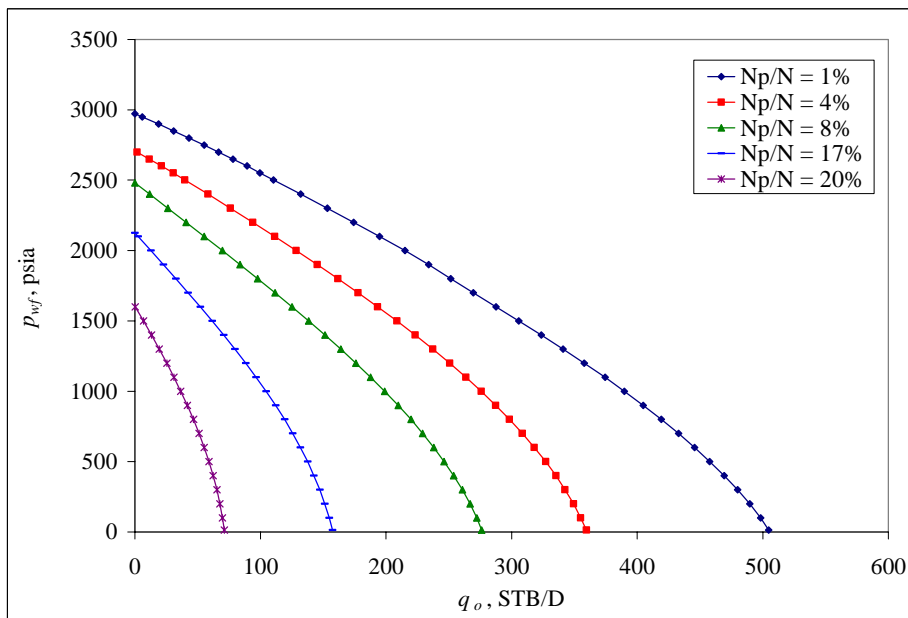


Fig. A-13 IPR curves for case 14 (refer to Table 2)

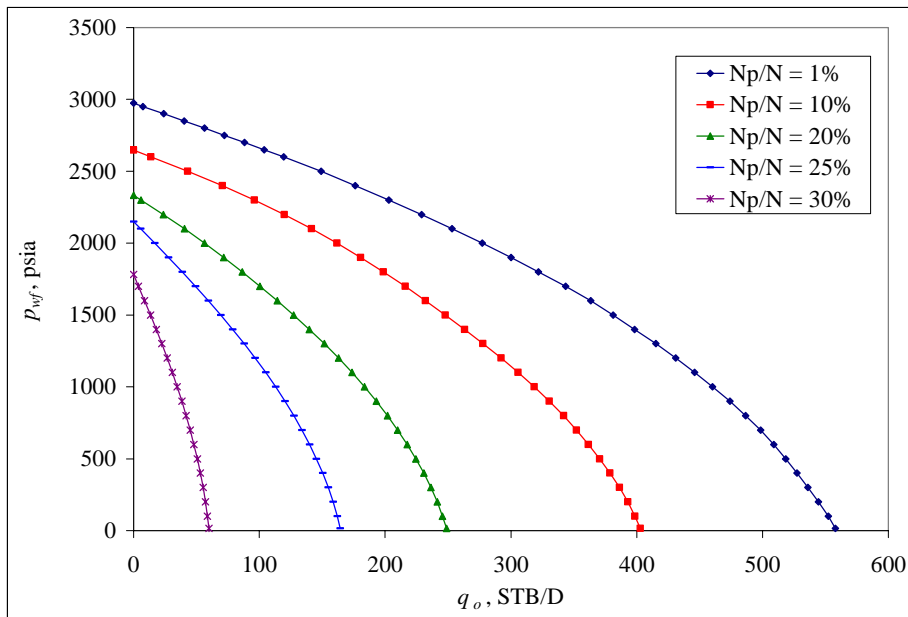


Fig. A-14 IPR curves for case 15 (refer to Table 2)

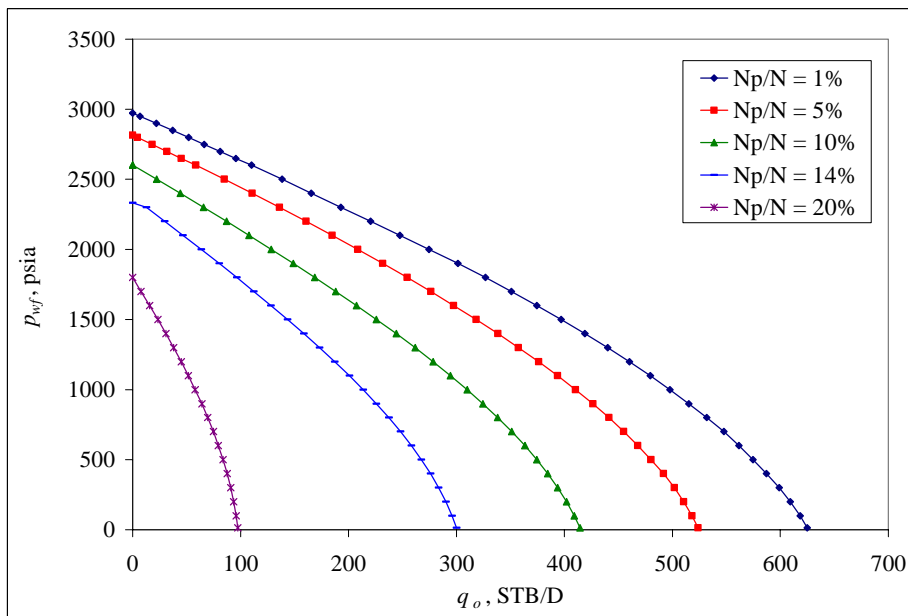


Fig. A-15 IPR curves for case 16 (refer to Table 2)

VITA

Name: Muhammad Alrumah
Born: 21 August 1976
Kuwait city, Kuwait
Permanent Address: Petroleum Engineering Technology Department
College of Technological Studies
P.O.BOX 42325 Shwakh 7065 Kuwait
Education: Kuwait University, Kuwait
Bachelor of Science Degree in Petroleum Engineering
December 1998
Texas A&M University, College Station, Texas, USA
Master of Science Degree in Petroleum Engineering
December 2003